



Stress signaling and cellular proliferation reverse the effects of mitochondrial mistranslation

Nicola Ferreira^{1,2}, Kara L Perks^{1,2}, Giulia Rossetti^{1,2}, Danielle L Rudler^{1,2}, Laetitia A Hughes^{1,2}, Judith A Ermer^{1,2}, Louis H Scott^{1,2}, Irina Kuznetsova^{1,2}, Tara R Richman^{1,2}, Vinod K Narayana³, Laila N Abudulai^{4,5,6}, Anne-Marie J Shearwood^{1,2}, Henrietta Cserne Szappanos⁷, Dedreia Tull³, George C Yeoh^{1,2,5}, Livia C Hool^{7,8}, Aleksandra Filipovska^{1,2,5,*}  & Oliver Rackham^{1,9,10,**} 

Abstract

Translation fidelity is crucial for prokaryotes and eukaryotic nuclear-encoded proteins; however, little is known about the role of mistranslation in mitochondria and its potential effects on metabolism. We generated yeast and mouse models with error-prone and hyper-accurate mitochondrial translation, and found that translation rate is more important than translational accuracy for cell function in mammals. Specifically, we found that mitochondrial mistranslation causes reduced overall mitochondrial translation and respiratory complex assembly rates. In mammals, this effect is compensated for by increased mitochondrial protein stability and upregulation of the citric acid cycle. Moreover, this induced mitochondrial stress signaling, which enables the recovery of mitochondrial translation via mitochondrial biogenesis, telomerase expression, and cell proliferation, and thereby normalizes metabolism. Conversely, we show that increased fidelity of mitochondrial translation reduces the rate of protein synthesis without eliciting a mitochondrial stress response. Consequently, the rate of translation cannot be recovered and this leads to dilated cardiomyopathy in mice. In summary, our findings reveal mammalian-specific signaling pathways that respond to changes in the fidelity of mitochondrial protein synthesis and affect metabolism.

Keywords metabolism; mitochondria; mitochondrial ribosome; protein synthesis; stress response

Subject Category Translation & Protein Quality

DOI 10.15252/embj.2019102155 | Received 1 April 2019 | Revised 17 September 2019 | Accepted 20 September 2019 | Published online 13 November 2019

The EMBO Journal (2019) 38: e102155

Introduction

Mitochondria are metabolic hubs of cells and house critical pathways for generating energy, purines, pyrimidines, ketone bodies, sex hormones, and iron–sulfur clusters, as well as being necessary for maintaining calcium and nitrogen balance (Pagliarini & Rutter, 2013). Consequently, the physiological function of mitochondria requires the production and folding of over 1,000 different proteins (Calvo & Mootha, 2010). The mitochondrial inner membrane is one of the most demanding sites for protein folding in the cell, where imported proteins must be folded immediately upon import and, in the case of the respiratory complexes, must assemble with a subset of proteins that are produced from a completely separate genome—the mitochondrial DNA (mtDNA) (Small *et al*, 2013). Therefore, the correct biogenesis of mitochondria depends on the production of balanced ratios of components from both genomes to assemble the multi-protein complexes within this organelle (Moehle *et al*, 2018). Mitochondrial damage and loss of function are hallmarks of aging, neurodegeneration, and myopathies (Vafai & Mootha, 2012; Riera *et al*, 2016). Mitochondria have their own, distinct, protein quality control systems that are poorly understood to date (Moehle *et al*, 2018). The proteins produced from the mitochondrial genome are indispensable for cellular energy production, and as such, mitochondrial protein synthesis is essential for life and defects in this process cause devastating diseases for which there are no cures or effective treatments, as well as contributing to cancer, diabetes, and neurological disorders (Murphy & Hartley, 2018). In contrast, decline in mitochondrial translation can induce a mitochondrial stress response and extend lifespan (Houtkooper *et al*, 2013). When the levels of unfolded mitochondrial proteins rise, they initiate a stress

1 Harry Perkins Institute of Medical Research, Nedlands, WA, Australia

2 The University of Western Australia Centre for Medical Research, Crawley, WA, Australia

3 Metabolomics Australia, Bio21 Institute of Molecular Science and Biotechnology, University of Melbourne, Parkville, Vic., Australia

4 Centre for Microscopy, Characterisation and Analysis, The University of Western Australia, Perth, WA, Australia

5 School of Molecular Sciences, The University of Western Australia, Crawley, WA, Australia

6 The School of Biomedical Sciences, The University of Western Australia, Nedlands, WA, Australia

7 School of Human Sciences (Physiology), The University of Western Australia, Crawley, WA, Australia

8 Victor Chang Cardiac Research Institute, Darlinghurst, NSW, Australia

9 School of Pharmacy and Biomedical Sciences, Curtin University, Bentley, WA, Australia

10 Curtin Health Innovation Research Institute, Curtin University, Bentley, WA, Australia

*Corresponding author: Tel: +61 8 6151 0735; E-mail: aleksandra.filipovska@uwa.edu.au

**Corresponding author: Tel: +61 8 6151 0736; E-mail: oliver.rackham@curtin.edu.au

response that signals to the nucleus in an effort to recover mitochondrial function (Higuchi-Sanabria *et al*, 2018). Although protein folding in mitochondria has been found to be of great importance, the role of fidelity of protein synthesis within mitochondria is not clear. Here, we introduced mutations to generate error-prone and hyper-accurate mitochondrial ribosomes (mitoribosome) in yeast and mice to test the importance of mistranslation on mitochondrial function and cell physiology.

As the ribosome traverses each mRNA, it reads 10–20 codons per second and incorporates the encoded amino acids into the growing polypeptide chain (Wohlgemuth *et al*, 2010). At each codon, the ribosome must screen numerous non-cognate and near-cognate tRNAs via kinetic proofreading to find the correct cognate tRNA (Zaher & Green, 2009). Such a demanding process necessitates higher error rates than DNA replication and transcription. Errors in translation fidelity occur when a tRNA is loaded with an incorrect amino acid or when ribosomes accept an incorrect interaction between an incoming tRNA and its corresponding codon in the mRNA template. The loading of incorrect amino acids onto tRNAs typically occurs because the chemical differences between some amino acids are very minor, and might consist of a single methyl or hydroxyl group. In the case of ribosomal errors, these occur because of the inherent competition between speed and accuracy in codon recognition (Zaher & Green, 2009). Over billions of years biological systems have found a trade-off that enables the massive demand for new proteins to be filled with an error rate that can be generally tolerated. However, this compromise does not appear to be optimized for all conditions (Mohler & Ibba, 2017).

A surprising theme that has emerged in recent years is that mistranslation can be beneficial and is actively induced in some situations (Moura *et al*, 2009). What could the benefits of mistranslation possibly be? The first is speed, if translation can accept a higher error rate, then the ribosome can work at a faster rate and produce more proteins in less time (Moura *et al*, 2009; Mohler & Ibba, 2017). The second benefit of mistranslation is that it can activate transcriptional stress responses; this primes the cell and enables it to survive a broad range of subsequent insults. Finally, mistranslation diversifies the cell's proteome providing new protein functions that can be advantageous in certain circumstances. For example, mistranslation that enables the production of proteins with a greater number of methionine residues can protect mammalian cells from oxidative stress (Netzer *et al*, 2009). Also, because the ribosome stabilizes and folds nascent polypeptides, as well as synthesizing them, diversity might be achieved at not just the primary structure level but also in terms of secondary and tertiary structure (Zhang & Ignatova, 2010).

Surprisingly, little is known about the role of translational fidelity in mitochondrial protein synthesis. Interestingly, a number of pathogenic mtDNA mutations have been proposed to impact the fidelity of translation (Suzuki *et al*, 2011); in particular, the A3243G mutation in mitochondrial tRNA^{Leu} associated with mitochondrial encephalopathy, lactic acidosis, and stroke-like episodes syndrome enables normal rates of translation but produces very unstable nascent chains, due to amino acid misincorporation (Sasarman *et al*, 2008). A recent study reported the introduction of error-prone and hyper-accurate mutations into the yeast mitoribosome and found that the error-prone mutants produced greater levels of reactive oxygen species and cytoplasmic protein aggregates that

activated a general stress response (Suhm *et al*, 2018). In contrast, the yeast with hyper-accurate mitoribosomes were protected from stresses. Here, we examined altered mitochondrial translation fidelity in mammals and found tissue-specific effects on the production of mitochondrial proteins and that, surprisingly, mitochondrial mistranslation can be compensated for by increased cellular proliferation and mitochondrial function could be restored with age. In contrast, high-fidelity translation could not be compensated for and resulted in cardiomyopathy.

Results

Hyper-accurate translation in yeast reduces mitochondrial function and *de novo* protein synthesis of mitochondria-encoded proteins

The mitoribosome descended from that of the original prokaryotic symbiont that evolved into modern-day mitochondria. As such, although they have changed in RNA and protein composition, particularly at the periphery, their core contains highly conserved proteins that are homologous to those of the bacterial ribosome (Greber & Ban, 2016). Therefore, to create ribosomes with altered fidelities we took advantage of mutations that have been discovered to result in error-prone or hyper-accurate translation in *Escherichia coli* (Agarwal *et al*, 2011). These were discovered via random mutagenesis of the *rpsL* gene, encoding the S12 protein of the small ribosomal subunit, which plays an important role in maintaining the fidelity of translation in prokaryotes during the tRNA selection process. The K43I and K42T substitutions in S12 were found to either increase or decrease amino acid misincorporation, respectively (Agarwal *et al*, 2011). These mutations affect amino acid positions that are completely conserved in the homologous proteins of the yeast and mammalian mitoribosomes, known as mitochondrial ribosomal protein of the small subunit 12 (MRPS12) or uS12m (Fig EV1A) (Greber & Ban, 2016). The equivalent mutations are at positions 71 and 72 of yeast and mouse MRPS12, such that the error-prone mutant is K72I and the hyper-accurate mutation is K71T. Recent structures of the mammalian and yeast mitoribosomes revealed that the loop containing these mutations forms a structurally conserved element of the decoding center in these ribosomes, as it does in bacteria, indicating that the mechanism of decoding is conserved (Fig 1A) (Amunts *et al*, 2015; Greber *et al*, 2015; Desai *et al*, 2017). To understand the effect of altering the fidelity of mitochondrial protein synthesis in yeast, we introduced both error-prone (*ep*, K72I) and hyper-accurate (*ha*, K71T) mutations into the *Saccharomyces cerevisiae* MRPS12 gene via homologous recombination (Fig EV1B).

We used a survival assay to determine whether alterations in translation fidelity in yeast affect the growth of yeast on different carbon sources. We found that the growth of MRPS12-K72I (*ep*) yeast on both fermentable and non-fermentable carbon sources was equal to that of MRPS12-WT yeast, suggesting that these yeast have intact mitochondrial respiration (Fig EV1C). In contrast, MRPS12-K71T (*ha*) yeast showed reduced growth with lactose and no growth with either glycerol or ethanol as carbon sources (Fig EV1C). This shows that MRPS12-K71T (*ha*) yeast are unable to use non-fermentable carbon sources, suggesting that they have impaired

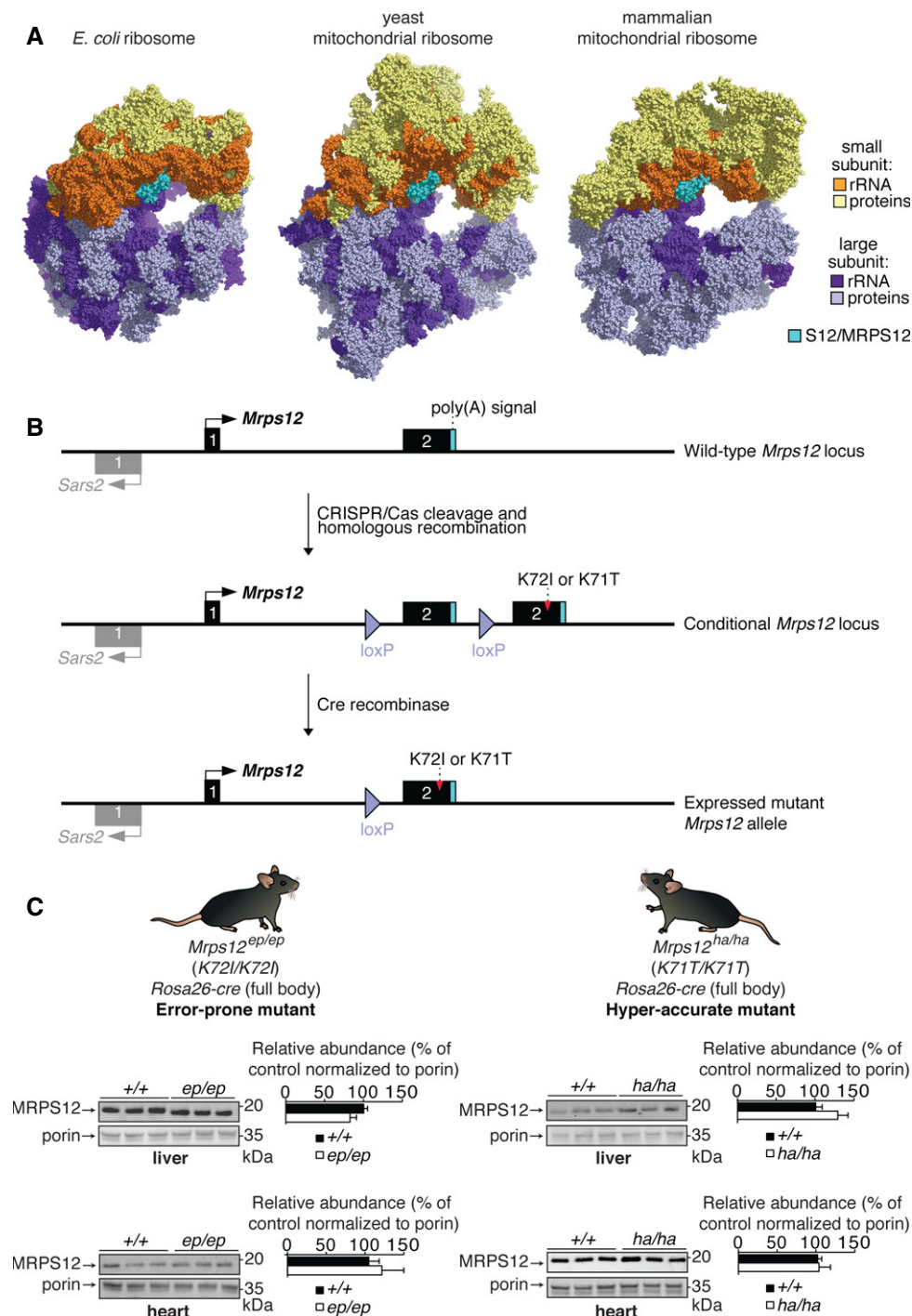


Figure 1. Models of error-prone and hyper-accurate mitochondrial translation.

A Structural comparison of the *Escherichia coli*, yeast mitochondrial, and mammalian mitochondrial ribosomes.
 B Schematic representation of the generation of the error-prone (*Mrps12*^{ep/ep}) and hyper-accurate (*Mrps12*^{ha/ha}) mouse models.
 C MRPS12 protein levels were determined in mitochondria isolated from livers and hearts from *Mrps12*^{+/+}, *Mrps12*^{ep/ep}, and *Mrps12*^{ha/ha} 10-week-old mice by immunoblotting. Porin was used as a loading control. Relative abundance of proteins was measured using Li-Cor Odyssey Classic software normalized to the loading control.

Data information: In (C), data are presented as mean ± SD. The data are representative of results obtained from six mice from each genotype.

mitochondrial respiration. Next, we used *de novo* pulse labeling to determine whether alterations in translation fidelity affect the rate of translation of newly produced polypeptides in yeast. We found no difference in the rate of protein synthesis in *MRPS12*-K72I (*ep*) yeast compared with *MRPS12*-WT yeast (Fig EV1D), while *MRPS12*-K71T (*ha*) yeast had reduced protein synthesis (Fig EV1D). The impaired rate of mitochondrial protein synthesis due to the *MRPS12*-K71T (*ha*) mutation likely explains their reduced growth on non-fermentable carbon sources and indicates that the hyper-accurate fidelity defect has a greater fitness cost than the error-prone translation defect in yeast.

Error-prone mitochondrial translation and hyper-accurate mitochondrial translation in mice are compatible with life

To further understand consequences of altered fidelities of mitochondrial protein synthesis on mitochondrial function and physiology *in vivo*, we generated error-prone (*ep*, K72I) and hyper-accurate (*ha*, K71T) mouse models. Because these mutations significantly alter the growth rate of *E. coli* (Agarwal *et al*, 2011) and the ability of yeast to grow on non-fermentable carbon sources, in the case of the K71T mutation, we were concerned that introducing them into the *Mrps12* gene might cause embryonic lethality in mice. Therefore, we produced conditional alleles, where the exon containing the point mutations was duplicated and placed after the transcription termination and polyadenylation signals of the native gene, such that it was not expressed (Fig 1B). We incorporated *loxP* sites flanking the native exon and transcription termination and polyadenylation signals, such that the Cre recombinase can be used to seamlessly replace the wild-type exon with a mutant exon. We bred both *Mrps12^{ep}* and *Mrps12^{ha}* alleles with *Rosa26-cre* mice that express the Cre recombinase ubiquitously to delete the wild-type copy of exon 2 in the germline and obtain heterozygous *Mrps12^{+/ep}* or *Mrps12^{+/ha}* animals. Intercrossing *Mrps12^{+/ep}* or *Mrps12^{+/ha}* mice produced *Mrps12^{+/+}*, heterozygote, and *Mrps12^{ep/ep}* or *Mrps12^{ha/ha}* pups in Mendelian proportions (genotyped pups $n = 224$, *Mrps12^{+/ep}* $n = 133$, *Mrps12^{+/+}* $n = 39$, and *Mrps12^{ep/ep}* $n = 52$; genotyped pups $n = 48$, *Mrps12^{+/ha}* $n = 24$, *Mrps12^{+/+}* $n = 10$, and *Mrps12^{ha/ha}* $n = 14$), demonstrating that both K71T and K72I mutations are compatible with life and both mutant mouse strains were initially indistinguishable from their wild-type littermates. Immunoblotting for the mitochondrial ribosomal protein, MRPS12, from the liver and heart mitochondria of *Mrps12^{+/+}* and *Mrps12^{ep/ep}* or *Mrps12^{ha/ha}* mice showed that homozygous mice have no differences in the levels of the MRPS12 protein compared with controls (Fig 1C). This confirms that alterations in the function, and not the level, of the MRPS12 protein underlie the phenotypes observed in these mice (see below).

Error-prone mitochondrial translation in mice reduces *de novo* protein synthesis of mitochondria-encoded proteins

We investigated if error-prone mitoribosomes affect the rate of protein synthesis in mice using *de novo* pulse and chase labeling. We examined 10- and 30-week-old animals because they represent adolescence and mature adulthood in mice. We found decreased translation of all mitochondria-encoded proteins in liver (Fig 2A) and heart mitochondria (Fig EV2A) of 10-week-old *Mrps12^{ep/ep}* mice

compared with controls, where the liver was more severely affected. This was not due to impaired mitoribosome biogenesis, as the abundance of the protein constituents of the small and large mitoribosomal subunits was not altered (Fig EV3A), nor was it due to impaired assembly or subunit association of the mutant mitoribosomes, as sucrose gradient fractionation profiles from livers of *Mrps12^{ep/ep}* and *Mrps12^{+/+}* mice were identical (Fig EV3B). Interestingly, although the mitochondrial translation initiation factors MTIF2 and MTIF3 were equally abundant in wild-type and *Mrps12^{ep/ep}* mice, the COXI-specific translational activator TACO1 was decreased in the liver at 10 weeks of age (Fig EV3C) but was increased at 30 weeks of age (Fig EV3C), indicating that translation fidelity has a specific impact on the efficiency of mitochondrial protein synthesis. To provide further evidence for the effect of the *Mrps12* mutation on translational accuracy, we performed pulse and chase *in organello* translation assays in the presence or absence of gentamicin, an antibiotic whose binding impairs translational proof-reading. In mitochondria from error-prone (*Mrps12^{ep/ep}*) mice, gentamicin had a strongly additive effect on inhibition of protein synthesis with the mutation compared with control mice (Fig EV3D). These results make sense in light of a compound defect when genetically induced mistranslation and drug-induced mistranslation are combined in *Mrps12^{ep/ep}* mitochondria, and confirm the underlying molecular effects on mitochondrial translation.

Slower cytoplasmic translation in yeast can destabilize mRNAs, resulting in reduced protein production (Presnyak *et al*, 2015). Northern blotting of mitochondrial mRNAs revealed that their levels were increased in the liver by the altered translation in *Mrps12^{ep/ep}* mice (Fig 2B); while levels of mitochondrial tRNAs were increased at 10 weeks of age in the hearts of *Mrps12^{ep/ep}* mice (Fig EV2B). In *E. coli*, reduced protein synthesis results in a rapid drop in tRNA abundance (Svenningsen *et al*, 2017); however, the opposite appears to be true in mammalian mitochondria, as knockouts of other proteins that affect translation have also been observed to have an increased abundance of tRNAs (Park *et al*, 2007; Cámara *et al*, 2011; Ruzzenente *et al*, 2012; Perks *et al*, 2018). Surprisingly, in aged, 30-week-old mice, mitochondrial translation had largely recovered and there was only a subtle reduction in the translation of all mitochondria-encoded proteins in the liver (Fig 2C) and heart mitochondria (Fig EV2C) of *Mrps12^{ep/ep}* mice compared with controls. This was accompanied by a concomitant normalization of mRNA and tRNA levels in the liver and heart, respectively, at 30 weeks of age (Figs 2D and EV2D). This shows that the liver is more affected by the consequences of error-prone translation but that with age the defects in the rate of translation of mitochondria-encoded proteins are ameliorated.

Error-prone translation in mice affects the steady-state levels of mitochondria-encoded proteins

We investigated the effects of mistranslation on mitochondria- and nuclear-encoded oxidative phosphorylation (OXPHOS) proteins by immunoblotting in both liver and heart mitochondria. We observed a reduction in the steady-state levels of NDUFB8 and the mitochondria-encoded COXI and COXII in the livers (Fig 2E) of 10-week-old *Mrps12^{ep/ep}* mice compared with *Mrps12^{+/+}* mice, while there were no differences in the steady-state levels of OXPHOS polypeptides in the heart mitochondria (Fig EV2E) of young *Mrps12^{ep/ep}* mice

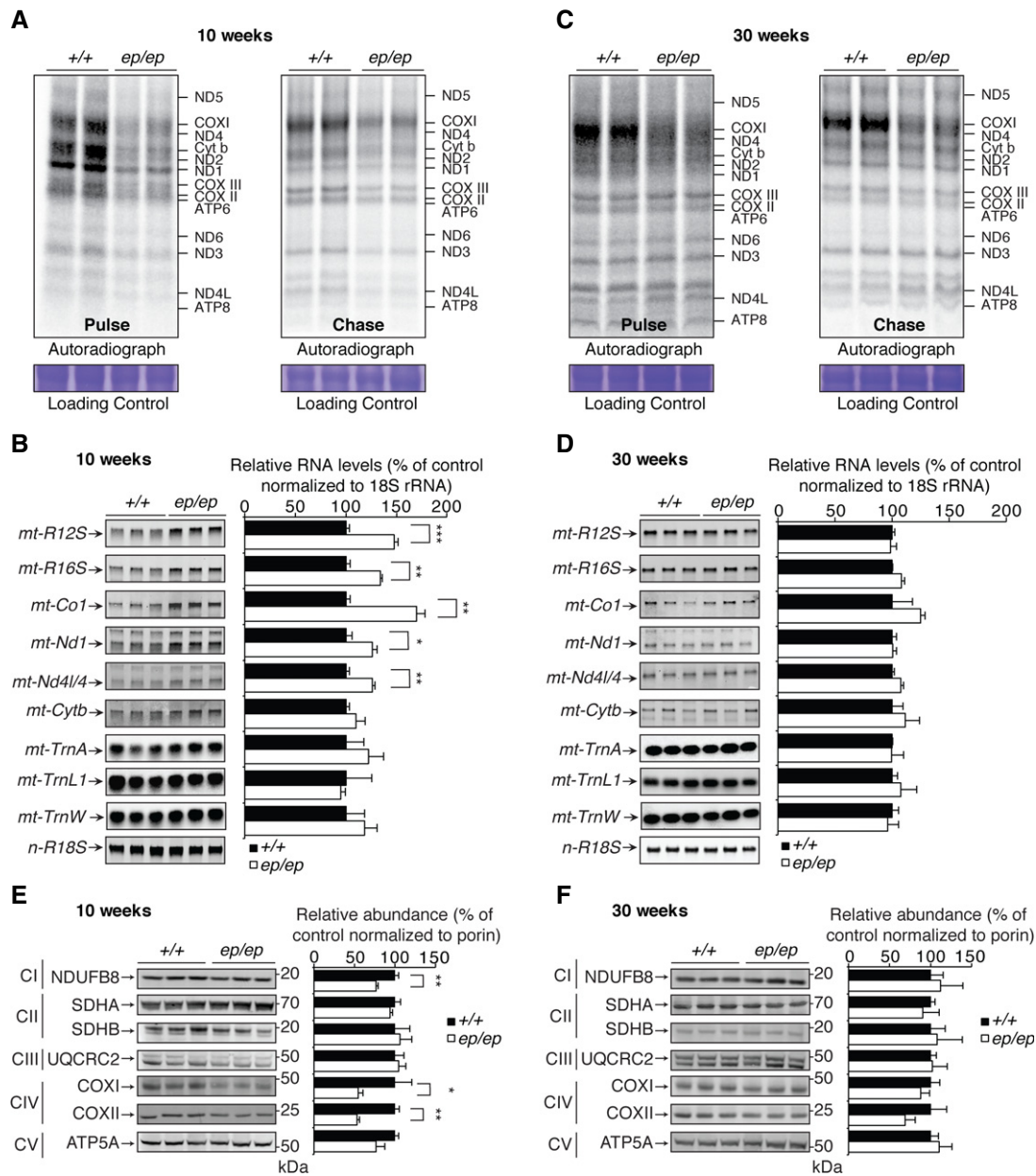


Figure 2. Error-prone mitochondrial translation reduces the rate of translation and the abundance of mitochondrial mRNAs and proteins but is rescued with age.

- A** *De novo* protein synthesis in mitochondria isolated from the livers of young (10-week-old) *Mrps12^{+/+}* and *Mrps12^{ep/ep}* mice was measured by pulse and chase incorporation of ³⁵S-labeled methionine and cysteine. Mitochondrial proteins were separated by SDS–PAGE, stained using Coomassie Brilliant Blue to show equal loading, and visualized by autoradiography.
- B** The steady-state levels of mature mitochondrial mRNAs, tRNAs, and rRNAs in liver of young (10-week-old) *Mrps12^{+/+}* and *Mrps12^{ep/ep}* mice were analyzed by northern blotting. 18S rRNA was used as a loading control. Relative abundance of RNA was measured using Li-Cor Odyssey Classic software normalized to the loading control.
- C** *De novo* protein synthesis in mitochondria isolated from the livers of aged (30-week-old) *Mrps12^{+/+}* and *Mrps12^{ep/ep}* mice was measured by pulse and chase incorporation of ³⁵S-labeled methionine and cysteine, as described in (A).
- D** The steady-state levels of mature mitochondrial mRNAs, tRNAs, and rRNAs in liver of aged (30-week-old) *Mrps12^{+/+}* and *Mrps12^{ep/ep}* mice were analyzed by northern blotting, as described in (B).
- E, F** Mitochondria isolated from livers of young (10-week-old, E) and aged (30-week-old, F) *Mrps12^{+/+}* and *Mrps12^{ep/ep}* mice were examined by immunoblotting using antibodies to investigate the steady-state levels of nuclear- and mitochondria-encoded OXPHOS polypeptides. Porin was used as a loading control. Relative abundance of proteins was measured using Li-Cor Odyssey Classic software normalized to the loading control.

Data information: In (A, C), autoradiographs and stained gels are representative of results obtained from six mice from each genotype. In (B, D, E, F), data are presented as mean \pm SD. * $P < 0.05$, ** $P < 0.01$, *** $P < 0.001$ (two-tailed paired Student's *t*-test). These data are representative of results obtained from eight mice from each genotype.

compared with controls. This shows that overall error-prone translation affects the synthesis of proteins but the steady-state protein levels are only decreased in the liver, which is more severely affected. The fact that the impact on the steady-state levels of mitochondrial respiratory complex subunits was not as severe as the defects on *de novo* protein synthesis indicates that these complexes were stabilized in an attempt to limit the impact of the defect in mitochondrial translation. In older, 30-week-old *Mrps12^{ep/ep}* mice, we found no differences in the abundance of OXPHOS proteins in the liver (Fig 2F) and heart mitochondria (Fig EV2F). This provides a further indication that with age *Mrps12^{ep/ep}* mice are able to correct for the decreased rate of translation caused by the error-prone mitoribosomes.

To understand the impact of error-prone translation on mitochondrial function and biogenesis, we measured oxygen consumption in liver and heart mitochondria to determine whether mitochondrial respiratory function was affected due to alterations in translation fidelity. Respiration was decreased in the liver but was not significantly decreased in heart mitochondria of 10-week-old mutant mice (Figs 3A and EV4A), consistent with the decreased protein synthesis rate and levels of mitochondria-encoded OXPHOS subunits. Mitochondrial oxygen consumption was recovered in 30-week-old *Mrps12^{ep/ep}* mice compared with controls (Figs 3A and EV4A). Next, we analyzed the levels of the mitochondrial respiratory complexes by blue native polyacrylamide gel electrophoresis (BN-PAGE) followed by immunoblotting for each respiratory complex. We observed reduced levels of OXPHOS complexes and significantly reduced levels of Complex IV in the liver mitochondria from 10-week-old *Mrps12^{ep/ep}* mice; however, there were no changes in the levels of respiratory complexes in the heart mitochondria and the levels normalized in the livers of 30-week-old *Mrps12^{ep/ep}* mice, compared with controls (Figs 3B and EV4B).

Altered respiratory complex assembly but not protein quality control in response to mitochondrial mistranslation

Next, we used *de novo* pulse labeling followed by BN-PAGE to determine whether alterations in translation fidelity affect the rate of assembly of newly synthesized respiratory complexes. We observed a decrease in the rate of assembly of mitochondria-encoded respiratory complexes in the liver of 10-week-old *Mrps12^{ep/ep}* mice compared with controls (Fig 3C), indicating that the reduced synthesis of mitochondria-encoded proteins reduces the assembly of respiratory complexes but that an increase in their stabilities enables the maintenance of their steady-state levels. These data indicate that the alternations in translation fidelity affect the OXPHOS levels and function early in life but these recover by 30 weeks of age.

Mitochondrial proteases are essential for protein quality control mechanisms as they are responsible for degrading misfolded and oxidatively damaged proteins in the mitochondrial matrix or inner mitochondrial membrane (Quirós *et al*, 2015). We used immunoblotting to determine the steady-state levels of proteases from the liver and heart mitochondria of *Mrps12^{ep/ep}* and *Mrps12^{+/+}* mice in response to altered translation fidelity. There were no differences in the steady-state levels of proteases in the liver and heart mitochondria of *Mrps12^{ep/ep}* mice compared with *Mrps12^{+/+}* mice (Figs 3D and EV4C). The lack of a response in mitochondrial

proteases is congruent with the increased stability of the mitochondria-encoded proteins and complexes.

Increased cellular proliferation and telomerase expression are activated by mitochondrial stress signaling

We examined the livers of 10- and 30-week-old *Mrps12^{ep/ep}* mice to explore how the translational defect could be recovered over time. We noted that the overall body weight and liver weight of the *Mrps12^{ep/ep}* mice tended to be increased compared with control mice but this was not significant (Fig 4A). Hematoxylin and eosin staining of the hearts of *Mrps12^{ep/ep}* mice at 10 and 30 weeks of age did not reveal any abnormalities (Fig EV4D), while histology of the livers revealed a dramatic increase in polyploid cells in the 30-week-old *Mrps12^{ep/ep}* mice by hematoxylin and eosin staining as well as Gomori trichrome staining (Fig 4B). We confirmed these observations by Hoechst 33342 fluorescent staining of nuclei in *Mrps12^{ep/ep}* liver sections (Fig 4C). Hepatocyte polyploidy has been hypothesized to be a result of high energy demands competing with cell proliferation during post-natal liver development or to enhance certain metabolic activities via increased gene copy number (Celton-Morizur *et al*, 2010). Immunohistochemistry of Ki67 as a proliferation marker revealed much greater cellular proliferation in the 30-week-old *Mrps12^{ep/ep}* liver sections (Fig 4C). These data show that mitochondrial mistranslation stimulates increased polyploidy and proliferation in the liver.

We examined cell signaling pathways that have previously been implicated in mitochondrial stress responses to understand how mitochondrial mistranslation stimulates increased liver proliferation. Total SAPK and the phosphorylated form were unchanged, but phospho-AKT levels were increased in the 30-week-old *Mrps12^{ep/ep}* livers compared with controls, consistent with the increase in hepatocyte proliferation but lack of inflammation (Fig 4D). The steady-state and phosphorylated form of mTOR was also unaffected in the 30-week-old *Mrps12^{ep/ep}* livers compared with controls (Figs 4D and EV4D), although its targets, S6 and phospho-S6 levels, and phospho-EBP1 were decreased in 30-week-old hearts of *Mrps12^{ep/ep}* mice (Fig EV4E).

We used qRT-PCR to examine the levels of mRNAs encoding proteins involved in liver proliferation and found an increase in mRNAs encoding β -catenin (*Ctnnb1*) and GSK3 β (*Gsk3b*) (Fig 4E). Unlike most cells in adult organs, a sub-population of liver cells expresses *Tert*, which encodes the catalytic subunit of telomerase, and these cells are responsible for liver maintenance and renewal (Lin *et al*, 2018). We found that *Tert* abundance was significantly increased in the 30-week-old *Mrps12^{ep/ep}* liver (Fig 4E), providing an explanation for the increased cellular proliferation we observed in these mice. To understand how mitochondrial dysfunction stimulates an increase in telomerase, we examined the expression of all transcription factors that are known to act on the *Tert* gene (Gładych *et al*, 2011). Although unchanged in the 10-week-old mutants, the expression of CEBP β , RELA, SP1, and HIF1 α (encoded by *Cebpb*, *Rela*, *Sp1*, and *Hif1a*) was significantly increased in the 30-week-old *Mrps12^{ep/ep}* livers (Fig 4E). The increase in transcription factors which act on the *Tert* gene explains the upregulation of *Tert* expression and cell proliferation.

Interestingly, one of CEBP β 's best characterized roles is as an initiating transcription factor of the mitochondrial stress response

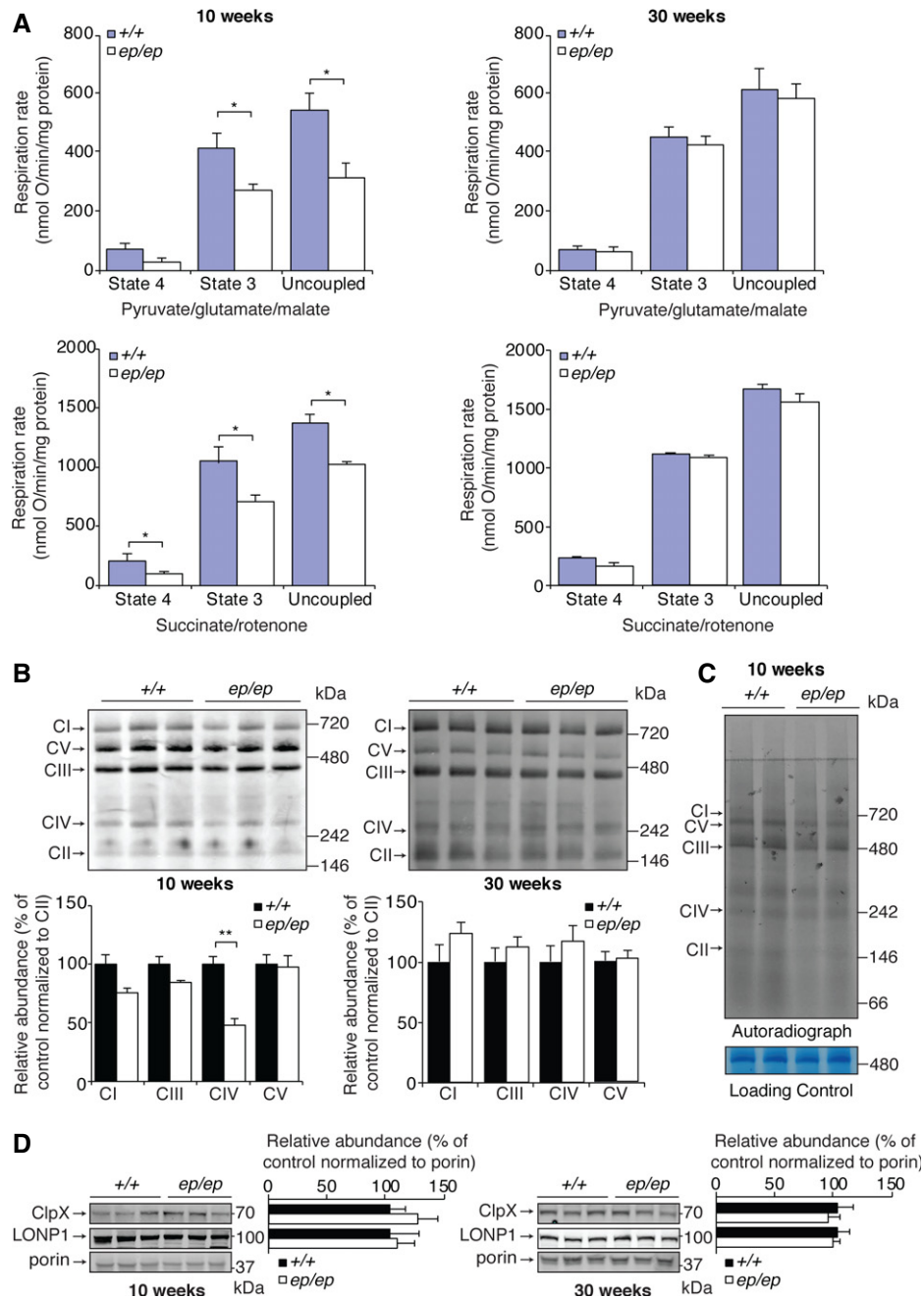


Figure 3. Error-prone mitochondrial translation reduces the rate of respiratory complex assembly and respiration but does not alter the levels of proteins involved in proteolysis.

- A Non-phosphorylating (state 4), phosphorylating (state 3), and uncoupled respiration in the presence of 2 μ M FCCP was measured in liver mitochondria isolated from *Mrps12^{+/+}* and *Mrps12^{ep/ep}* mice using an OROBOROS oxygen electrode using either pyruvate, glutamate, and malate as substrates or with succinate in the presence of rotenone at 10 weeks or 30 weeks of age.
- B Isolated liver mitochondria were resolved by BN-PAGE and immunoblotted using the blue native OXPHOS antibody cocktail. Relative abundance of proteins was measured using Li-Cor Odyssey Classic software normalized to Complex II.
- C The rates of respiratory complex assembly were measured by pulse incorporation of ³⁵S-labeled methionine and cysteine. Equal amounts of mitochondrial protein were separated by BN-PAGE, stained using Coomassie Brilliant Blue to show equal loading, and visualized by autoradiography.
- D Proteins from liver mitochondria of young (10-week-old) and aged (30-week-old) *Mrps12^{+/+}* and *Mrps12^{ep/ep}* mice were immunoblotted using antibodies to investigate the steady-state levels of nuclear-encoded proteases. Porin was used as a loading control. Relative abundance of proteins was measured using Li-Cor Odyssey Classic software normalized to the loading control.

Data information: In (A), data are presented as mean \pm SD. * $P \leq 0.05$ (Student's *t*-test). The data are representative of results obtained from eight mice from each genotype. In (B, D), data are presented as mean \pm SD. ** $P \leq 0.01$ (Student's *t*-test). The data are representative of results obtained from six mice from each genotype. In (C), the autoradiograph and stained gel are representative of results obtained from six mice from each genotype.

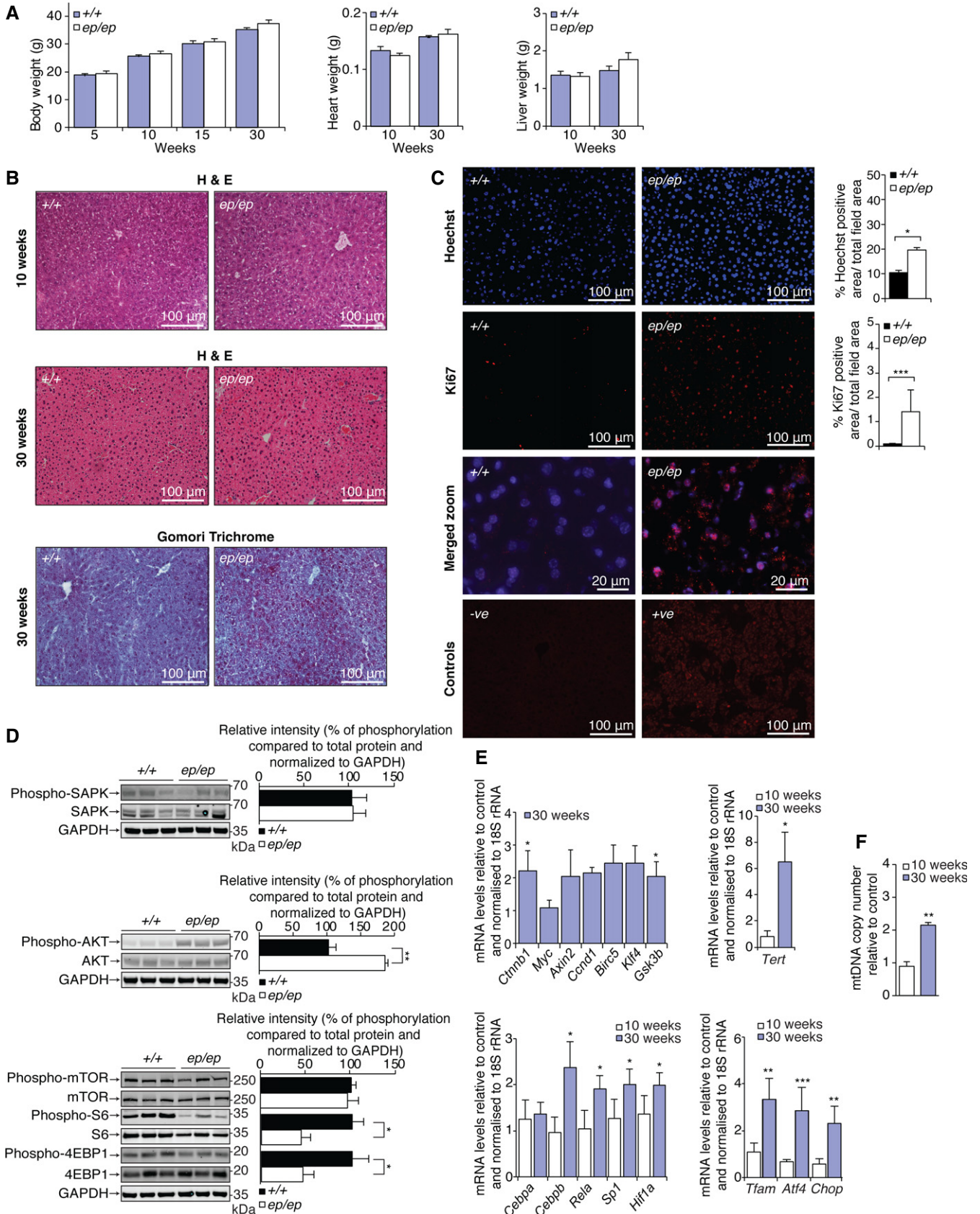


Figure 4.

Figure 4. Error-prone mitochondrial translation stimulates liver proliferation via a transcriptional response that induces telomerase expression and mitochondrial biogenesis.

- A The body, heart, and liver weights of *Mrps12^{+/+}* and *Mrps12^{ep/ep}* mice at 5, 10, 15, and 30 weeks of age.
 B Liver sections from young (10-week-old) and aged (30-week-old) *Mrps12^{+/+}* and *Mrps12^{ep/ep}* mice were stained with hematoxylin and eosin (H & E) or Gomori's trichrome and visualized at 20× magnification. Scale bar is 100 μm.
 C Liver sections from 30-week-old *Mrps12^{+/+}* and *Mrps12^{ep/ep}* mice were stained with Hoechst 33342 dye or against an antibody to Ki67 and visualized using fluorescence microscopy at 20× magnification; the scale bar is 100 μm. Merged images were taken at 40× magnification, and the scale bar is 20 μm. Normal liver and tumor sections were used as negative and positive controls, respectively. Percent of fluorescent positive area within sections was calculated using NIS Elements AR software (Nikon).
 D Cellular proteins from the livers of 30-week-old *Mrps12^{+/+}* and *Mrps12^{ep/ep}* mice were immunoblotted to investigate the steady-state levels of SAPK, AKT, and mTOR signaling proteins and their phosphorylated forms. GAPDH was used as a loading control, and the relative abundance of phosphorylated proteins was measured using Li-Cor Odyssey Classic software normalized to total protein, relative to the loading control.
 E Quantitative RT-PCR was used to measure the abundance of mRNAs encoding proteins involved in liver proliferation, the catalytic subunit of telomerase (*Tert*), transcription factors that regulate *Tert* expression, and proteins that regulate mitochondrial biogenesis (*Tfam*, *Atf4*, *Chop*). The data were normalized to 18S rRNA.
 F Mitochondrial DNA (mtDNA) was measured using quantitative PCR, and values were normalized to the β-2-microglobulin (*B2m*) gene.

Data information: In (A), data are presented as mean ± SD of results obtained from 10 mice from each genotype. In (B, C), images are representative of results obtained from six mice from each genotype. In (C–F), data are presented as mean ± SD of results obtained from six mice of each genotype. **P* ≤ 0.05, ***P* ≤ 0.01, ****P* ≤ 0.001 (two-tailed paired Student's *t*-test).

(Zhao *et al*, 2002). We examined the downstream effectors of the mitochondrial stress response, CHOP, ATF4, and TFAM, and found that they also significantly increased in expression (Fig 4E). TFAM abundance is typically found to correlate with mtDNA levels (Ekstrand *et al*, 2004; Jiang *et al*, 2017), which we also found to be increased in the 30-week-old *Mrps12^{ep/ep}* mice (Fig 4F). Therefore, recovery of mitochondrial function in the face of mitochondrial mistranslation is accomplished by increases in both mitochondrial biogenesis and cellular proliferation that are activated in tandem by the mitochondrial stress response.

Citric acid cycle activity is altered in response to mitochondrial mistranslation

We performed metabolite profiling of *Mrps12^{ep/ep}* liver mitochondria from 10- and 30-week-old mice and found significant increases in citric acid cycle intermediates, including citrate, isocitrate, succinate, and malate as well as certain fatty acids, compared with controls at 10 weeks of age (Fig 5A). The increase in citric acid cycle activity may be a compensatory response in an effort to maintain electron flow. The induction of the mitochondrial citric acid cycle has been previously reported to metabolically enable mitochondrial dysfunction and cause oxidative stress during hepatic insulin resistance (Satapati *et al*, 2012). Interestingly, we also observed a significant increase in cholesterol in the mitochondria from 10-week-old *Mrps12^{ep/ep}* mice (Fig 5A), which may result from the increased levels of citrate, as has been observed previously (Parlo & Coleman, 1984). However, by 30 weeks of age *Mrps12^{ep/ep}* mitochondria have normalized levels of citric acid cycle intermediates and cholesterol, indicating that the recovery of mitochondrial translation also enables the normalization of mitochondrial metabolism.

To understand the mechanisms that enable error-prone translation to be compensated for at the molecular level, we performed proteomic analyses of wild-type and *Mrps12^{ep/ep}* liver mitochondria. Gene ontology enrichment analyses revealed that the most affected proteins included those important for mitochondrial metabolic processes involved in ATP production, and that these alterations were dampened at 30 weeks of age (Fig 5B). This confirms the importance of the citric acid cycle alterations we observed in

the metabolite profiling and revealed the important enzymes involved, as citric acid cycle enzyme subunits of isocitrate dehydrogenase (IDH3G), fumarylacetoacetate hydrolase (FAH), succinyl-CoA:glutarate-CoA transferase (SUGCT), succinate dehydrogenase (SDHA, SDHB), and malate dehydrogenase (MDH1) were altered in abundance in *Mrps12^{ep/ep}* liver mitochondria (Fig 5C). Many subunits of the respiratory chain complexes were decreased in the 10-week-old *Mrps12^{ep/ep}* mice (Fig 5C); however, by 30 weeks of age the levels of the majority of these had normalized in *Mrps12^{ep/ep}* mitochondria relative to controls, further confirming the recovery of mitochondrial translation and respiratory complex assembly.

High-fidelity mitochondrial translation in mice progressively reduces *de novo* protein synthesis of mitochondria-encoded proteins and causes cardiomyopathy

Given the physiological impact of error-prone mitochondrial translation, we investigated if improved translational fidelity could also impact cell and organ function in mice. First, we examined whether hyper-accurate mitoribosomes affect the rate of protein synthesis in mice using *de novo* pulse and chase labeling. We found that the level and rate of translation of mitochondria-encoded proteins in heart and liver mitochondria of 10-week-old *Mrps12^{ha/ha}* mice were only subtly affected compared with controls (Figs 6A and EV5A). At 30 weeks of age, we observed mild defects in the synthesis and stability of mitochondria-encoded proteins in the heart (Fig 6A) but not the liver mitochondria of *Mrps12^{ha/ha}* mice compared with controls (Fig EV5A). This shows that hyper-accurate translation has a more subtle effect on protein synthesis and stability in young mice in comparison with error-prone translation. In addition, the effect of gentamicin addition was almost entirely buffered in pulse labeling of hyper-accurate (*Mrps12^{ha/ha}*) mitochondrial translation, compared with the error-prone translation that was almost completely eliminated (Fig EV3D), confirming the hyper-accurate phenotype of the *Mrps12^{ha/ha}* ribosomes.

The minor changes in *de novo* translation in the *Mrps12^{ha/ha}* mice did not significantly alter the steady-state levels of mitochondria-encoded proteins in liver (Fig EV5B) and heart (Fig 6B) mitochondria of 10-week-old *Mrps12^{ha/ha}* mice compared with controls;

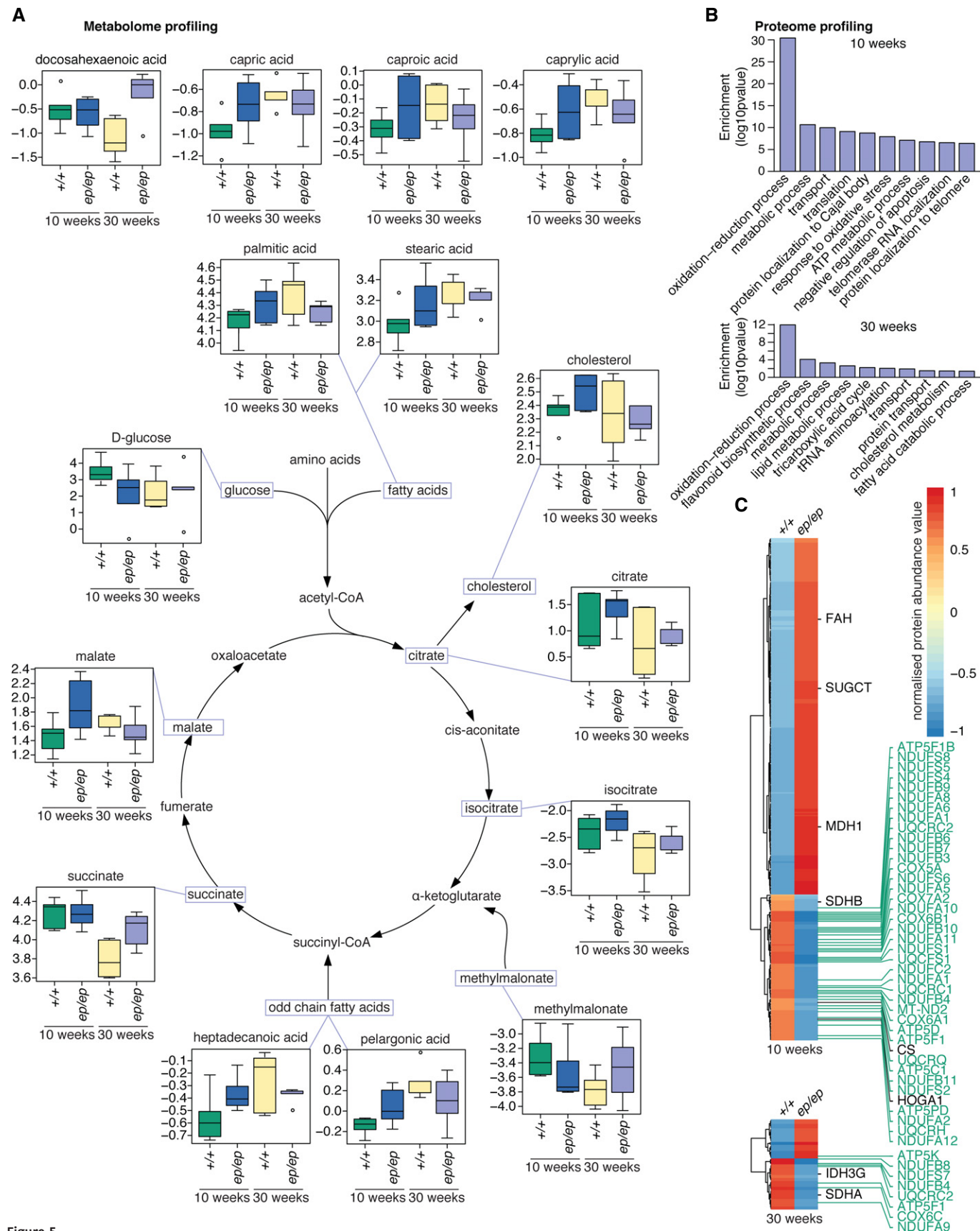


Figure 5.

Figure 5. Citric acid cycle metabolites and enzymes are altered in response to mitochondrial mistranslation.

- A Metabolite profiling revealed alterations in the citric acid cycle that normalizes with age.
 B Proteomic analyses of samples from 10- and 30-week-old *Mrps12*^{+/+} and *Mrps12*^{ep/ep} mice revealed an enrichment in proteins that are involved in citric acid cycle-related biological processes, by gene ontology analyses. Detailed CirGO graphs (Kuznetsova et al, 2019) of enriched biological processes are provided in Appendix Figures S1 and S2.
 C Respiratory chain subunit proteins and citric acid cycle enzymes that were altered in abundance are labeled in green and black, respectively, within a heatmap of all significantly altered proteins within the proteomic dataset.

Data information: In (A), data are presented as box plots of the fold change (x-axis) of metabolites; horizontal middle lines represent the mean, and the box ranges are the upper and lower quartiles, with the whiskers showing the highest and lowest observations of results obtained from five to six mice from each genotype. Only metabolites whose abundance was significantly changed between *Mrps12*^{+/+} and *Mrps12*^{ep/ep} mice, after Benjamini–Hochberg correction (FDR 0.01), are graphed. Samples were normalized according to median signal intensity. In (B, C), data are results obtained from five mice of each genotype, with averages presented in (C).

however, these levels were reduced in the hearts of 30-week-old *Mrps12*^{ha/ha} mice (Fig 6B). Similarly, there were no significant changes in mitochondrial respiration in the livers of 30-week-old *Mrps12*^{ha/ha} mice (Fig EV5C) and the body and liver weights of these mice did not differ from wild-type controls (Fig EV5D and E). However, there was significant decrease in oxygen consumption in heart mitochondria from 30-week-old *Mrps12*^{ha/ha} mice compared with controls (Fig 6C) and the sizes of their hearts were significantly decreased (Fig 6D–F). Echocardiography revealed that 30-week-old *Mrps12*^{ha/ha} mice had altered cardiac morphology and function consistent with the development of dilated cardiomyopathy (Fig 6G). This included a significant decrease in fractional shortening, and a significant increase in diastolic and systolic diameters, as well as dilated chamber size, compared with control mice. Hematoxylin and eosin staining showed an increase in cardiomyocyte size, cellular disarray, and increased presence of necrotic foci in 30-week-old hearts from *Mrps12*^{ha/ha} mice (Fig 6H), further demonstrating the development of cardiomyopathy in these mice.

Unlike the error-prone (*Mrps12*^{ep/ep}) mice, in the hyper-accurate (*Mrps12*^{ha/ha}) mice the disease phenotype progressed with age and did not reverse. Therefore, we examined cellular signaling pathways to understand the differences between the two responses to altered mitochondrial translation fidelity. Total AKT was unaltered in the hearts of *Mrps12*^{ha/ha} mice but was increased in their livers; however, the phosphorylated form of AKT was unchanged in the heart (Fig EV5F). The mTOR target, S6, and phospho-S6 were decreased in both the hearts and livers of 30-week-old *Mrps12*^{ha/ha} mice (Fig EV5F). Since these changes in S6 were seen in tissues without disease, they are unlikely to be critical to the pathology. However, the *Mrps12*^{ha/ha} mice did not mount the same transcriptional response as the error-prone mice (Fig EV5G). Notably, the expression of mitochondrial stress response genes *Chop*, *Atf4*, and *Tfam* was not upregulated (Fig EV5G) and the mtDNA levels did not change (Fig EV5H). Proteomic analyses of wild-type and *Mrps12*^{ha/ha} heart mitochondria revealed that proteins involved in cardiac and mitochondrial metabolic processes were most enriched (Fig EV5I). Subunits of the respiratory chain complexes were significantly decreased in the 30-week-old *Mrps12*^{ha/ha} mouse hearts (Fig EV5J), confirming the defects in synthesis of mitochondria-encoded proteins, and the downstream consequences for complexes consisting of these, in mice with hyper-accurate mitochondrial translation. The lack of a full transcriptional mitochondrial stress response likely underlies the inability of the heart to recover from the translational dysfunction imposed by the *Mrps12*^{ha/ha} mutation.

Discussion

The protein sequences encoded in our genomes have been extensively honed by evolution since life began over 3.5 billion years ago. Therefore, maintaining the accuracy of these sequences during DNA replication, transcription, and translation is critical to the function of all biological systems. DNA replication is highly accurate, with errors only occurring every 1 in 10⁸ nucleotides, while transcription (1 error every 10⁵ nucleotides) and translation (1 error every 10³–10⁵ amino acids) are much more error prone (Mohler & Ibba, 2017). In fact, on average, about 14% of all synthesized proteins are estimated to contain at least one missense amino acid substitution (Parker, 1989). How cells cope with this issue remains to be clarified. Here, we show that yeast with error-prone protein synthesis have equal growth and translation rates to that of wild-type yeast whereas yeast harboring hyper-accurate mitoribosomes have reduced growth and translation rates, consistent with what has been observed in *E. coli* mutants (Agarwal et al, 2011). However, unlike the *E. coli* mutants and the yeast model, error-prone mitochondrial protein synthesis in mice causes a dramatic reduction in the rate of translation of proteins in both liver and heart mitochondria.

The exact mechanism that results in reduced translation in mice expressing error-mitoribosomes is not clear but could result from missense amino acid misincorporations that cause co-translational stalling. Mitoribosomes could be more sensitive to these changes due to the highly specialized nature of the polypeptide exit tunnel, co-translational docking, and membrane insertion that occur for mitochondria-synthesized proteins (Kummer et al, 2018), where inappropriate protein folding could interfere. Nevertheless, despite the severe reduction in *de novo* mitochondrial protein synthesis early in life due to error-prone mitochondrial translation, the steady-state levels of mitochondrial transcripts are increased, likely in an attempt to compensate for the reduction in newly synthesized polypeptides. Due to the alteration in mitochondrial translation and despite the increase in mitochondria-encoded RNA, we found that the steady-state levels of mitochondria-encoded OXPHOS polypeptides were decreased early in life. Consequently, the function and biogenesis of mitochondria was reduced, but not enough to cause pathology. This suggests that mitochondria have a high tolerance for mistranslated proteins and unknown mechanisms exist to respond to the defect by stabilizing the assembled respiratory complexes.

Metabolic studies have previously been performed in cases of severe mitochondrial dysfunction and have found that one-carbon metabolism, proline synthesis, and coenzyme Q biogenesis are

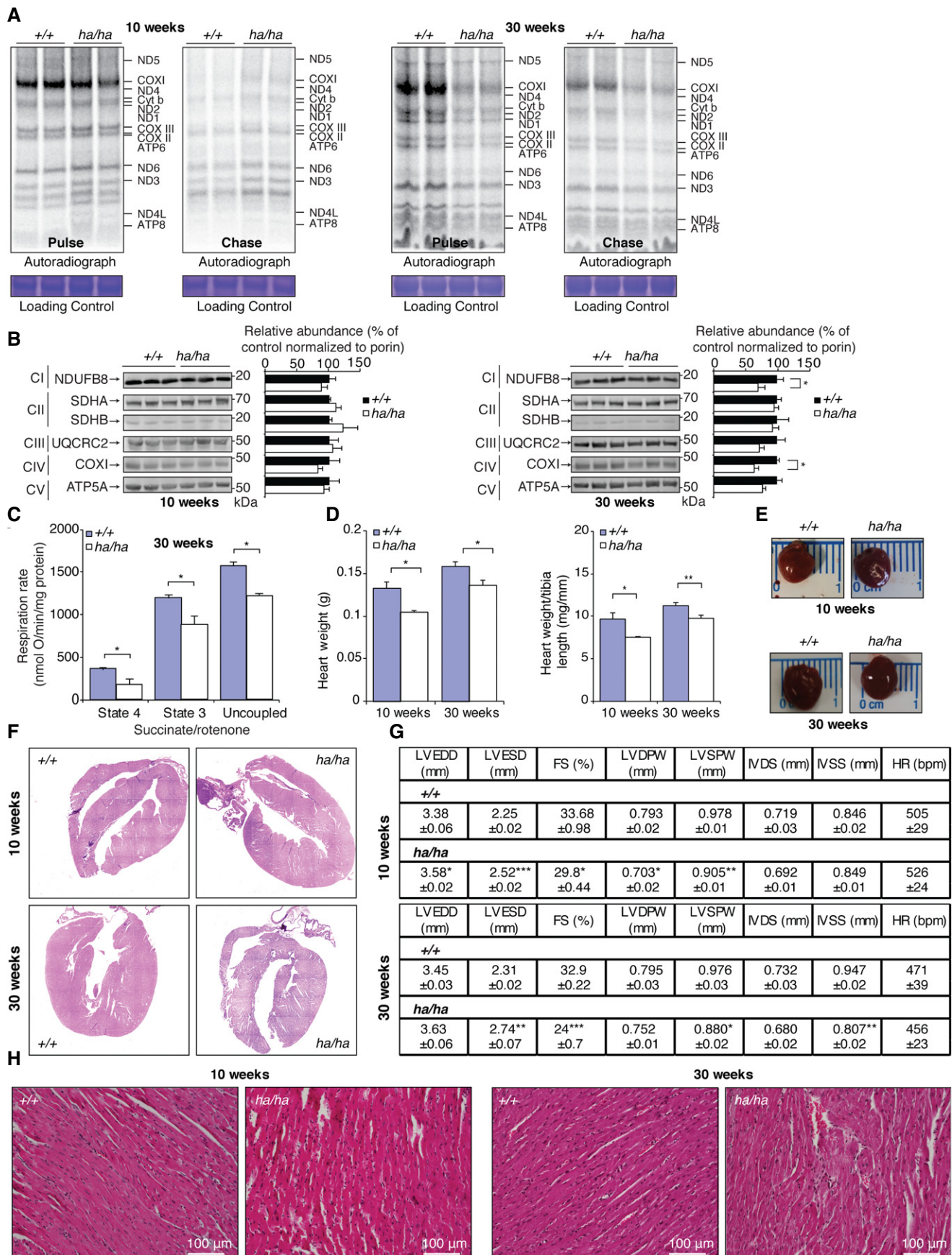
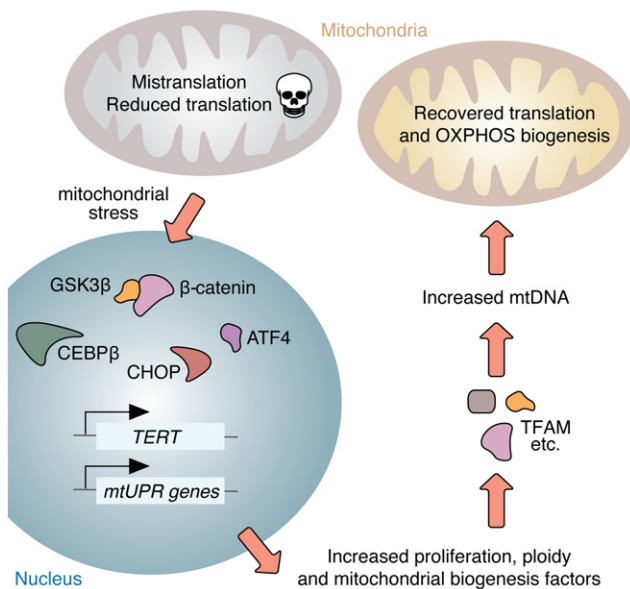


Figure 6.

Figure 6. Hyper-accurate mitochondrial mistranslation reduces mitochondrial respiration and results in a progressive dilated cardiomyopathy.

- A *De novo* protein synthesis in mitochondria isolated from the hearts of young (10-week-old) and aged (30-week-old) *Mrps12^{+/+}* and *Mrps12^{halha}* mice was measured by pulse and chase incorporation of ³⁵S-labeled methionine and cysteine. Mitochondrial proteins were separated by SDS-PAGE, stained using Coomassie Brilliant Blue to show equal loading, and visualized by autoradiography.
- B Mitochondrial proteins from the hearts of young (10-week-old) and aged (30-week-old) *Mrps12^{+/+}* and *Mrps12^{halha}* mice were immunoblotted using antibodies to investigate the steady-state levels of nuclear- and mitochondria-encoded OXPHOS polypeptides. Porin was used as a loading control. Relative abundance of proteins was measured using Li-Cor Odyssey Classic software normalized to the loading control.
- C Non-phosphorylating (state 4), phosphorylating (state 3), and uncoupled respiration in the presence of 2 μ M FCCP was measured in heart mitochondria isolated from *Mrps12^{+/+}* and *Mrps12^{halha}* mice using an OROBOROS oxygen electrode using succinate in the presence of rotenone at 30 weeks of age.
- D Differences in heart weight between *Mrps12^{+/+}* ($n = 10$) and *Mrps12^{halha}* ($n = 10$) mice at 10 and 30 weeks of age. Values are also shown relative to tibia length.
- E Images of representative hearts from *Mrps12^{+/+}* and *Mrps12^{halha}* mice at 10 and 30 weeks of age.
- F Histology of hematoxylin and eosin (H & E) stained heart cross-sections from young (10-week-old) and aged (30-week-old) *Mrps12^{+/+}* and *Mrps12^{halha}* mice, visualized at 10 \times magnification, and individual images were assembled using Adobe Photoshop.
- G Echocardiographic parameters for *Mrps12^{+/+}* ($n = 8$) and *Mrps12^{halha}* 10-week-old and 30-week-old mice. LVEDD, left ventricular end-diastolic diameter; LVESD, left ventricular end-systolic diameter; FS, fractional shortening; LVDPW, left ventricular posterior wall in diastole; LVSPW, left ventricular posterior wall in systole; IVDS, intraventricular septum in diastole; IVSS, intraventricular septum in systole; HR, heart rate.
- H Heart sections cut to 5- μ m thickness were stained with H & E from young (10-week-old) and aged (30-week-old) *Mrps12^{+/+}* and *Mrps12^{halha}* mice and visualized at 20 \times magnification. Scale bar is 100 μ m.

Data information: In (A), autoradiographs and stained gels are representative of results obtained from six mice from each genotype. In (B, C), data are presented as mean \pm SD of results obtained from six mice from each genotype. In (D), data are presented as mean \pm SD of results obtained from 10 mice from each genotype. In (E, F, H), images are representative of results obtained from six mice from each genotype. In (G), data are presented as mean \pm SD of results obtained from eight mice of each genotype. * $P \leq 0.05$, ** $P \leq 0.01$, *** $P \leq 0.001$ (two-tailed paired Student's *t*-test).

**Figure 7. Mitochondrial stress signaling and cellular proliferation rescue mitochondrial mistranslation.**

A model illustrating how a transcriptional response to low-level mitochondrial stress can mitigate the effects of mitochondrial mistranslation by activating cell proliferation and mitochondrial biogenesis.

significantly altered in these models (Bao *et al*, 2016; K \ddot{u} hl *et al*, 2017). However, in our model which exhibits mild mitochondrial dysfunction these metabolic pathways were not significantly rewired. Instead, citric acid cycle metabolism was increased in response to error-prone translation in 10-week-old mice, likely in an effort to maintain electron flow through the respiratory complexes. Massive changes in metabolites in knockout models with severe mitochondrial dysfunction probably overestimate the number of metabolites that contribute to mitochondrial stress signaling, and

our model suggests that a few metabolites likely activate the broad transcriptional and proteomic changes seen in mitochondrial stress responses.

Surprisingly, with age there is a correction in the translation rate in mitochondria from mice expressing error-prone mitoribosomes with normalization of protein synthesis, mitochondrial RNA abundance, and steady-state protein levels by 30 weeks of age. We found that this is due to a compensatory response initiated by a transcriptional activation of the mitochondrial stress response master regulator CEBP β , which acts to increase mitochondrial biogenesis in concert with ATF4 and CHOP via TFAM but also by increasing cellular proliferation in the liver via increased telomerase expression (Fig 7). This is a previously unreported transcriptional response that appears to be distinct from the post-transcriptional signaling pathways that increase mitochondrial biogenesis in response to energy demands (Morita *et al*, 2013) or that upregulate telomerase in response to increased mitochondrial biogenesis (Wang *et al*, 2018), as both of these act via the mTOR pathway, that is not activated by the low levels of stress that result from mitochondrial mistranslation in our model. Post-transcriptional responses are more rapid than transcriptional responses and are better suited to deal with extreme stresses, while the transcriptional responses we observe are potentially better suited to improve the stability of mitochondrial function over a longer timeline.

CEBP β , ATF4, and CHOP are also key activators of the mitochondrial unfolded protein response (mtUPR) (Higuchi-Sanabria *et al*, 2018; Moehle *et al*, 2018); however, we did not observe significant upregulation of mitochondrial proteases in the *Mrps12^{ep/ep}* mice, perhaps due to a simultaneous induction of systems that stabilize mitochondrial respiratory complexes, as we observed in these mice at 10 weeks of age. We and others have previously observed increased ATF4 and CHOP in mouse models with impaired mitochondrial translation (Rackham *et al*, 2016; Seiferling *et al*, 2016; Perks *et al*, 2018), and impaired mitochondrial translation can induce mtUPR in worms and mammalian cell culture (Houtkooper *et al*, 2013). In contrast, loss of the Lon protease in flies activates mtUPR and inhibits mitochondrial translation (Pareek *et al*, 2018)

and the downstream targets of mtUPR include mitochondrial translation in mammalian cell culture (Münch & Harper, 2016). These observations highlight the distinct systems of nuclear-mitochondrial signaling in mammals and the need for further studies to understand how mitochondrial stress response programs bifurcate under different stresses.

Interestingly, the recovery of mitochondrial function in the liver is accompanied by an increase in polyploidy. Polyploidy is a distinctive phenomenon in the liver that occurs during post-natal development as an age-dependent process, but is also a hallmark of repair in response to injury and in response to various stress stimuli. Although not associated with membrane fission, polyploidy occurs due to substantial DNA replication followed by nuclear fusion and results in increased biosynthetic activity, hence the significant increase in Ki67 staining revealing DNA replication that would result in hyperplasia and/or hypertrophy, with either increasing the metabolic capacity of the liver. In most other tissues, this would result in increased cell numbers but in liver this can result from proliferation (karyokinesis) without membrane division (cytokinesis). Recent studies have shown that polyploid hepatocytes increase the expression of most genes associated with RNA metabolism, with protein and RNA transport, as well as genes involved in biosynthesis of purine nucleotides, ribosomes, amino acids, and fatty acids (Kreutz *et al*, 2017). Therefore, the unique properties of the liver might provide an advantage to recover from mitochondrial dysfunction.

Cell proliferation appears to be one of the responses that rescues mitochondrial dysfunction in response to mitochondrial mistranslation; however, post-natal proliferation does not occur in many tissues. Therefore, tissues such as the heart, that are mainly post-mitotic, could be more sensitive than the liver to minor mitochondrial dysfunction, explaining the progressive disease seen in the hyper-accurate mitochondrial translation mutant mice. In addition, the metabolic function of the liver, whose mitochondria are hubs for more diverse reactions that involve the citric acid cycle, might enable the increased citric acid cycle metabolites found in the early disease phenotype seen in the error-prone mitochondrial translation model. The citric acid cycle in liver is not intimately linked to β -oxidation, since excess acetyl-CoA can be used to make ketones and non-oxidative pathways can be used for gluconeogenesis, lipogenesis, and ureagenesis (Owen *et al*, 2002). Therefore, reduced respiratory capacity could increase fluxes in the citric acid cycle, as we observed during the peak of mitochondrial dysfunction in the error-prone mitochondrial translation mice. Although the unique metabolic properties of liver mitochondria may enable the rewiring of the citric acid cycle in an attempt to compensate for mitochondrial dysfunction, it would not provide an ideal solution to the problem as increased flux through the citric acid cycle would likely result in oxidative stress, and this cannot explain the subsequent recovery of mitochondrial function as the citric acid cycle metabolites normalize in the 30-week-old mice.

Contemporaneously with our presented work, another study reported the introduction of error-prone and hyper-accurate MRPS12 mutations into yeast and saw the same growth defects as in our yeast models (Suhm *et al*, 2018). Further study of an error-prone mutant (P50R) revealed the accumulation of protein aggregates and activation of a general transcriptional stress response. In contrast to what we observed in mice, the yeast harboring the error-prone MRPS12 mutation could not compensate for the mitochondrial

translation defect and exhibited concurrent failure of cytoplasmic proteostasis that decreased their lifespan (Suhm *et al*, 2018). The disparate phenotypes observed in yeast and mice highlight the diverse signaling and transcriptional responses available in mammalian systems compared with yeast. The transcriptional program observed in yeast is a generic Msn2/4-driven stress response that is also initiated when yeast are exposed to many different stresses, including starvation, osmotic stress, oxidative stress, and temperature stress (Görner *et al*, 2002; Hasan *et al*, 2002; Kandror *et al*, 2004). The ability of mammalian systems to specifically detect and respond to mitochondrial stress in a more specific way enables the consequences of mitochondrial mistranslation to be compensated for with time, via specific transcriptional upregulation of particular genes to increase mitochondrial biogenesis and cellular proliferation, and potentially harnessing tissue-specific programs such as polyploidy of the liver.

In contrast to error-prone mitoribosomes, hyper-accurate mitoribosomes in mice cause only a small reduction in mitochondrial protein synthesis in the heart, consistent with the *E. coli* mutants and yeast models (Agarwal *et al*, 2011; Suhm *et al*, 2018). Hyper-accurate translation results in slightly lowered overall levels of mitochondrial proteins that do not have defects, and consequently, mitochondrial stress response pathways are not activated to rescue protein synthesis, and OXPHOS function is ultimately compromised, resulting in cardiomyopathy. There must be a threshold for mitochondrial translation rate where the error-prone mutants activate the observed stress response that is not reached by the hyper-accurate mutant mitoribosomes. Therefore, it appears that mitochondrial translation rate is more important than translational accuracy, in terms of the ultimate physiological consequences for these mice. It is interesting to note that error-prone mitochondrial translation has more deleterious consequences in yeast (Suhm *et al*, 2018), while hyper-accurate mitochondrial translation has a greater physiological impact in mice. Mice carrying a V338Y mutation in the Mrps5 gene have also been recently shown to have increased mitochondrial mistranslation; interestingly, these mice exhibited enhanced anxiety and were more susceptible to noise-induced hearing loss (Akbergenov *et al*, 2018). Taken together, these studies demonstrate that the effects of altered translation fidelity differ between organisms and may highlight the distinct systems that have developed in these rapidly evolving organelles between yeast and mammals. Future studies could take advantage of the distinct stress responses between mitochondria of different organisms to elucidate the cell signaling molecules and networks that enable different mitochondrial defects to be compensated for, paving the way for targeted therapies for mitochondrial diseases and disorders where mitochondrial dysfunction is a key contributor.

Materials and Methods

Yeast strains

Saccharomyces cerevisiae CK (*MAT α* , *leu1*, *kar1-1*) was grown and maintained on yeast peptone adenine dextrose (YPAD) media or agar (1% w/v yeast extract, 2% w/v peptone, 2% w/v glucose, 0.05% w/v ammonium sulfate, 0.004% w/v adenine sulphate and 2% agar). A homology-directed repair (HDR) template was

generated by cloning the *S. cerevisiae* *MRPS12* ORF and 100 bp of 3' flanking sequence into the *SacI* and *XbaI* sites 5' of the kanMX expression cassette of pUG6. The resulting plasmid was subsequently used to clone 192 bp of *MRPS12* 3' flanking sequence 3' of the kanMX cassette via *SacI* and *SacII*. K72I and K71T mutations were introduced into the HDR template using QuikChange mutagenesis. Sequence-verified point mutants of the HDR template plasmid and a wild-type control were linearized using *SacI* and *SacII* and transformed into the CK strain as described by Gietz and Woods (2006). G418-resistant colonies were analyzed by PCR and Sanger sequencing to verify the correction genomic insertion of the HDR cassette and the integrity of the point mutations.

Yeast survival assay

Overnight cultures of yeast were resuspended in Tris-EDTA (TE) buffer (10 mM Tris, 1 mM EDTA, pH 8) at 1 OD₆₀₀ unit/ml. Each yeast suspension was used to make 1/10 serial dilutions in TE buffer, and five microliters of each dilution was inoculated as standing droplets on yeast peptone (YP) agar plates containing either 2% glucose, 3% acetate, 2% lactose and 0.1% glucose, 2% lactose, 2% glycerol, or 2% ethanol as carbon sources. The plates were imaged after 2–3 days of growth at 30°C.

Yeast mitochondrial isolation and *de novo* translation assays

Yeast were grown in YPAD medium, and mitochondria were isolated as described by Glick and Pon (1995). Protein concentration was measured using the BCA assay with BSA as a standard. *De novo* mitochondrial translation assays were performed according to Gouget et al (2008).

Transgenic mice

ES cells with an *Mrps12*^{ep} conditional allele were generated by Cyagen Biosciences. Briefly, a *Mrps12* gene-targeting vector was generated using mouse genomic fragments amplified from BAC clones with high-fidelity Taq DNA polymerase that were assembled into a plasmid together with recombination sites and selection markers, as indicated in Fig 2, and confirmed by Sanger sequencing. The resulting vector was linearized using *NotI* and electroporated into C57BL/6N ES cells. G418 was used for positive selection, and the diphtheria toxin subunit A gene was used for negative selection. Correctly targeted ES cell clones were identified using long-range PCR, expanded, and subjected to Southern blotting to confirm proper targeting by both homology arms. ES cell clones were microinjected into donor blastocysts, followed by transfer into surrogate mothers to obtain chimeric offspring, which were bred with wild-type C57BL/6N mice to generate germline F1 heterozygote mice, as verified by PCR and Sanger sequencing.

Mice carrying the *Mrps12*^{ep} conditional allele (*Mrps12*^{+ /ep-neo}) were used to produce a *Mrps12*^{ha} conditional allele via CRISPR-mediated homologous recombination. A homology-directed repair (HDR) template oligonucleotide was designed to repair the *Mrps12*^{ep} point mutation while simultaneously introducing the *Mrps12*^{ha} point mutation and incorporating 60 nt of flanking homology at either end (5'-CCACAGAGGGCCGGCCCAAGCTGAAGGGTGTGGTGTTCGCACATTCATCCGAAAGCCGACCAAGCCCAACTCCGCCAACCGCAA

GTGCTGCCGAGTCCGCCTCAGCACAGGCAAAGAGGCTGTC-3') was obtained from IDT. A single-guide RNA (gRNA) with the protospacer element sequence 5'-ACTTGCGGTTGGCGGAGTTG-3' was synthesized from plasmid templates containing the T7 promoter using the HiScribe T7 Quick High Yield RNA Synthesis Kit (NEB). RNAs were purified using the RNeasy Mini Kit (Qiagen). *In vitro* transcribed sgRNA, Cas9 mRNA (Sigma), and HDR oligonucleotide were microinjected into embryos derived from the *Mrps12*^{+ /ep-neo} mice and transferred into the uteri of pseudopregnant females. Genomic DNA from F0 and F1 animals was extracted from tail tips, and primers flanking genomic regions of interest were used in PCRs; amplicons were cloned and Sanger sequenced to confirm the integrity of the introduced genetic modification.

The neomycin cassette was removed by mating *Mrps12*^{+ /ep-neo} and *Mrps12*^{+ /ha-neo} mice with transgenic mice ubiquitously expressing Flp recombinase. The resulting *Mrps12*^{+ /ep} and *Mrps12*^{+ /ha} mice were mated with mice ubiquitously expressing Cre recombinase to generate heterozygous mutant *Mrps12*^{+ /ep-Cre} and *Mrps12*^{+ /ha-Cre} mice that were bred with each other to generate homozygous mutant mice without the *Rosa26-Cre* transgene and to identify that the homozygous mutation of *Mrps12* was not embryonic lethal. Age- and litter-mate-matched wild-type (*Mrps12*^{+ /+}) and homozygous (*Mrps12*^{ep/ep} or *Mrps12*^{ha/ha}) mice were housed in standard cages (45 cm × 29 cm × 12 cm) under a 12-h light/dark schedule (lights on 7 am to 7 pm) in controlled environmental conditions of 22 ± 2°C and 50 ± 10% relative humidity and fed a normal chow diet (Rat & Mouse Chow, Specialty Foods, Glen Forrest, Western Australia), and water was provided *ad libitum*. All animals were euthanized by cervical dislocation in the morning (between 8 and 9 am) to avoid circadian variation. The study was approved by the Animal Ethics Committee of the UWA and performed in accordance with Principles of Laboratory Care (NHMRC Australian Code for the Care and Use of Animals for Scientific Purposes, 8th Edition 2013).

Mitochondrial isolation

Mitochondria were collected from homogenized hearts and livers and isolated by differential centrifugation as described previously (Rackham et al, 2016) with some modifications. Livers were homogenized in buffer containing 250 mM sucrose, 5 mM Tris, and 1 mM EGTA, pH 7.4 with EDTA-free Complete protease inhibitor cocktail (Roche), and hearts were homogenized in buffer containing 210 mM mannitol, 70 mM sucrose, 10 mM Tris, and 0.1 mM EDTA pH 7.4 with EDTA-free Complete protease inhibitor cocktail (Roche) before differential centrifugation. The mitochondrial protein concentration was quantified using the BCA assay using BSA as a standard.

Proteomics

Mitochondrial proteins (100 µg) were resuspended in lysis buffer (6 M guanidinium chloride, 2.5 mM tris(2-carboxyethyl)phosphine hydrochloride, 10 mM chloroacetamide, and 100 mM Tris-HCl). After lysis, samples were diluted 1:10 in 20 mM Tris-HCl pH 8.0 and 100 µg of protein was mixed with 1 µg of Trypsin Gold (Promega) and incubated overnight at 37°C to achieve complete digestion. Peptides were cleaned with home-made STAGETips (Empore Octadecyl C18; 3M) and eluted in 60% acetonitrile/0.1% formic acid buffer. Samples were dried in a SpeedVac apparatus

(Eppendorf concentrator plus 5305) at 45°C, and the peptides were suspended with 0.1% formic acid; 1.2 µg of peptides was analyzed by LC-MS/MS.

For mass spectrometric analysis, digested peptides were loaded onto a trapping column (PepMap 100, C18, 100 mm × 2 cm) at a flow rate of 8 µl/min with 0.1% formic acid in water for 8 min before being separated on an analytical column (EASY-spray PepMap C18 column 75 µm × 50 cm, 2 mm bead diameter column; Thermo Fisher Scientific) using a Dionex UltiMate 3000 Nano-UHPLC system (Thermo Fisher Scientific). The column was maintained at 50°C. Buffers A and B were 0.1% formic acid in water and 0.1% formic acid in acetonitrile, respectively. Peptides were separated on a segmented gradient from 3 to 10% buffer B for 8 min, from 10 to 25% buffer B for 44 min, from 25 to 40% buffer B for 10 min, and from 40 to 95% buffer B for 12 min and equilibration (3% B) for 12 min, at 300 nl/min. Eluting peptides were analyzed on an Orbitrap Fusion Mass Spectrometer (Thermo Fisher Scientific). The instrument was operated in a data dependent, “Top Speed” mode, with cycle times of 2 s. The “Universal Method” template was used with some modifications. Peptide precursor mass-to-charge ratio (m/z) measurements (MS1) were carried out at 60,000 resolution in the 300–1,500 m/z range. The MS1 AGC target was set to $1e^6$ and maximum injection time to 300 ms. Precursor priority was set to “Most intense”, and precursors with charge states 2–7 only were selected for HCD fragmentation. Fragmentation was carried out using 27% collision energy. The m/z of the peptide fragments was measured in the orbitrap using an AGC target of $5e^4$ and 40 ms of maximum injection time.

Data from the Orbitrap Fusion (v 3.0.2041) were processed using Proteome Discoverer software, version 2.3 (Thermo Scientific). Peptide and protein identification was performed using Sequest HT against the UniProtKB *Mus musculus* database (UP00000589, release-2018_11). Sequest HT parameters included trypsin as a proteolytic enzyme, two missed cleavages allowed, minimum peptide length 6, peptide mass tolerance of 10 ppm, and a fragment mass tolerance of 0.02 Da. Peptide spectral match error rates were determined using the target-decoy strategy coupled to Percolator modeling of positive and false matches. Data were filtered at the peptide spectral match level to control for false discoveries using a q -value cut off = 0.01, as determined by Percolator. The normalization parameters in the Proteome Discoverer workflow were selected as follows: (i) The “normalization mode” was “total peptide amount”; (ii) “scaling mode” was “none”; (iii) “protein abundance calculation” was the “summed abundances”; (iv) “protein ratio calculation” was “protein abundance based”; and (v) “hypothesis test” was “ANOVA (individual proteins)”. The resulting file contained normalized master protein abundance values, where proteins with P -value < 0.05 were considered significant. In order to categorize the identified proteins, enriched Gene Ontology terms were identified using DAVID v.6.8 and summarized with REVIGO (Huang *et al*, 2009; Supek *et al*, 2011). Protein abundance results were visualized with Pheatmap v1.0.12 (R v. 3.5.3; 2019-03-11), where biological replicate values were averaged (Kolde, 2019).

Metabolomics

Frozen liver samples were weighed into cryomill tubes, and 1 ml of 3:1 methanol:water (v/v) solvent containing three internal standards

(13C5, 15N1 Valine [16 µM], 13C6-Leucine [6 µM], and 13C6-Sorbitol [6 µM]) was added. Samples were homogenized by cryogenic grinding using a precellys bead mill with a cryolys attachment (Bertin Technologies). Metabolites were extracted by adding 100 µl chloroform to each 400 µl of homogenate, and insoluble material was removed by centrifugation at 16,100 g (Beckman Coulter Microfuge 22R refrigerated microcentrifuge) for 10 min and the supernatant transferred to fresh tube. One hundred microliters of each supernatant was dried completely using a SpeedVac vacuum concentrator at 37°C (Christ RVC 2-33). Methoxyamine hydrochloride (20 µl; 30 mg/ml in pyridine) and 20 µl of BSTFA + 1% TMCS (Thermo Fisher Scientific) were used to derivatize the samples. Samples were analyzed by targeted multiple reaction monitoring (MRM) methodology from the Shimadzu Smart Metabolites Database, which contains MRM transitions for 475 metabolites using a GC-QQQ (TQ8040, Shimadzu Corporation) MS platform. Pooled biological quality controls (PBQC) were created for quality control monitoring during MS analysis by pooling extracts (50 µl) from individual study samples, and 100 µl was dried to make each PBQC. PBQCs were run at intervals of every five samples, while the order of all other samples was randomized. A total of 139 metabolites, including the three internal standards, were detected. Samples were normalized according to the median signal intensity, and Benjamini–Hochberg correction was applied to correct for the false positives.

Sucrose gradient fractionation

Sucrose gradient subfractionation was carried out as previously described (Richman *et al*, 2016). 1 mg of mitochondria was lysed in 1% *n*-dodecyl β-D-maltoside (Sigma). Lysates were loaded on 10–30% sucrose gradients and separated by centrifugation overnight as previously described (Ruzzenente *et al*, 2012; Rackham *et al*, 2016). Gradient fractions were collected as 750 µl aliquots and precipitated with trichloroacetic acid, resolved by SDS–PAGE, and ribosome-containing fractions were detected by immunoblotting using antibodies specific for individual proteins as described below.

RNA isolation and northern blotting

Total RNA was isolated from livers and hearts using the Qiagen miRNeasy Mini kit incorporating an on-column RNase-free DNase digestion to remove all DNA. RNA (4 µg) was resolved on 1.2% agarose formaldehyde gels, followed by transfer to 0.45 µm Hybond-N⁺ nitrocellulose membrane (GE Lifesciences) and hybridization with biotinylated oligonucleotide probes that specifically detect mouse mitochondrial mRNAs, rRNAs, and tRNAs (Rackham *et al*, 2016). All hybridizations were performed overnight at 50°C in 5× SSC, 20 mM Na₂HPO₄, 7% SDS, and 100 µg/ml heparin, followed by three 10-min washes. Hybridized oligos were detected using a streptavidin-linked infrared-labeled antibody (diluted 1:2,000 in 3× SSC, 5% SDS, 25 mM Na₂HPO₄, pH 7.5) using an Odyssey Infrared Imaging System (Li-Cor).

Immunoblotting

Proteins (50 µg) were resolved on 4–12% Bis-Tris gels, and specific proteins were detected using rabbit monoclonal antibodies against:

MRPS34 (HPA042112-100 μ l) and MRPL12 (HPA042112-100 μ l; Sigma – Prestige Antibodies, diluted 1:1,000); MRPS12 (14795-1-AP), MRPS35 (16457-1-AP), MRPL44 (16394-1-AP), MRPL37 (15190-1-AP), and MRPS16 (16735-1-AP; Proteintech, diluted 1:1,000); GAPDH (14C10), S6 ribosomal protein (5G10), phospho-S6 ribosomal protein (Ser235/236) (2F9), mTOR (7C10), phospho-mTOR (Ser2448) (D9C2), and 4E-BP1 (53H11); and phospho-4E-BP1 (Thr37/46) (236B4), SAPK, phospho-SAPK (Thr183/Tyr185) (81E11), AKT (C67E7), and phospho-AKT (Thr308) (244F9; Cell Signaling Technologies, diluted 1:500). Specific rabbit polyclonal antibodies were used against: LONP1 (15440-1-AP) and TACO1 (21147-1-AP; Proteintech, diluted 1:500); ClpX (HPA040262, Sigma – Prestige Antibodies, diluted 1:500); MTIF2 (LS-C164664/56970, LSBio, diluted 1:1,000); and MTIF3 (14219-1-AP, Proteintech, diluted 1:1,000). Specific mouse monoclonal antibodies used were as follows: Total OXPHOS Cocktail Antibody (ab110413, Abcam, diluted 1:5,000); porin (ab14734) and SDHA (ab14715; Abcam, diluted 1:1,000); and COXI (ab14705) and COXII (ab198286; Abcam, diluted 1:500). Antibodies were incubated in Odyssey Blocking Buffer (Li-Cor), and IR Dye 800CW Goat Anti-Rabbit IgG or IRDye 680LT Goat Anti-Mouse IgG (Li-Cor) secondary antibodies were used for detection, and the immunoblots were visualized using an Odyssey Infrared Imaging System (Li-Cor).

Blue native PAGE

Isolated mitochondria (80 μ g) were treated with 1% *n*-dodecyl β -D-maltoside and resolved on blue native 4–16% Bis-Tris gels, as described previously (Mourier *et al*, 2014). BN-PAGE gels were analyzed by transferring to PVDF and immunoblotting against respiratory complexes.

Respiration

Mitochondrial respiration was evaluated as oxygen consumption in isolated liver and heart mitochondria as previously described (Rackham *et al*, 2016). Mitochondria were supplemented with substrates 10 mM glutamate/2 mM malate/5 mM pyruvate (Sigma) or 10 mM succinate with the addition of the inhibitor 0.5 μ M rotenone (Sigma) to measure ADP-independent respiration activity (state 4). The addition of 1 mM ADP (Sigma) to the recording chamber was used to measure state 3 respiration activity. Respiration was uncoupled by successive addition of FCCP up to 3 μ M to reach maximal respiration.

Echocardiography

Echocardiography (ECG) was performed on mice under light methoxyflurane anesthesia with the use of an i13L probe on a Vivid 7 Dimension (GE Healthcare) as described before (Perks *et al*, 2017).

Histology

Fresh isolated hearts and livers were immediately incubated in 10% neutral buffered formalin for 24 h, followed by washing in phosphate-buffered saline and stored in 70% ethanol. Heart and liver tissues were embedded in paraffin and sectioned using a microtome, and the tissue sections were transferred to positively charged slides. The slides were heated for 2 h at 60°C and treated with xylene,

xylene and ethanol (1:1), and decreasing concentrations of ethanol (100, 95, 80, 60%) before they were washed in distilled H₂O. The H & E staining was performed as described before (Richman *et al*, 2015). Coverslips were mounted on slides using DPX mounting media (Scharlau), and images were acquired using a Nikon Ti Eclipse inverted microscope using a Nikon 20 \times objective.

Translation assay

In organello translation assays were carried out in isolated heart and liver mitochondria as described before (Rackham *et al*, 2016). Briefly, 500 μ g mitochondria were incubated in 750 μ l translation buffer (100 mM mannitol, 10 mM sodium succinate, 80 mM KCl, 5 mM MgCl₂, 1 mM KPi, 25 mM HEPES pH 7.4, 5 mM ATP, 20 μ M GTP, 6 mM creatine phosphate, 60 μ g/ml creatine kinase, and 60 μ g/ml of all amino acids except cysteine and methionine). Mitochondria were supplemented with 150 μ Ci of ³⁵S cysteine and methionine (PerkinElmer) for 60 min at 37°C. For chase experiments, after labeling, mitochondria were washed three times and incubated for 1 h at 37°C in translation buffer including cysteine and methionine. After labeling or chase, mitochondria were washed in translation buffer and suspended in 1% Triton X-100. Protein concentration was measured, and 50 μ g for liver and 25 μ g for heart of mitochondrial protein were resolved by SDS-PAGE and visualized by autoradiography.

Statistical analyses

All immunoblots were quantified using the Li-Cor Odyssey Classic software. All data with the exception of metabolomic data were statistically evaluated by a two-tailed paired Student's *t*-test and at a significance level of **P* \leq 0.05, ***P* \leq 0.01, or ****P* \leq 0.001 using Excel (Microsoft) and presented as mean \pm standard deviation. Metabolomic data were subjected to statistical analysis where the metabolites' abundance was measured as area under the observed peak that defines a metabolite. These data were pre-treated before statistical analysis to account for biological, experimental, and instrument variations by performing a natural log-transformation followed by normalizing the data to the median metabolic abundance of each sample and are presented as the mean, interquartile range, and the highest and lowest observations. In addition, Benjamini–Hochberg correction was applied to correct for the false positives with a false discovery rate of 0.01. The above statistical tests were performed using an in-house Metabolomics R package and MetaboAnalyst.

Data availability

Proteomics data are available from PRIDE with project accession number PXD015456 (<https://www.ebi.ac.uk/pride/archive/projects/PXD015456>).

Expanded View for this article is available online.

Acknowledgements

This project was supported by fellowships and project grants from the National Health and Medical Research Council (APP1156747 and APP1159594).

to AF and OR), Australian Research Council (DP170103000 to AF and OR), and the Cancer Council of Western Australia (to AF and OR). TRR is a CSIRO Future Fellow, Bright Spark Foundation Honorary Fellow, and Raine Foundation Grant recipient. NF, KLP, GR, DLR, LAH, and IK were supported by Australian Post-graduate Awards, and KLP was supported by the Mito Foundation. We thank the Children's Hospital Oakland Research Institute (CHORI) for providing the mouse chromosome 7 BAC clones (RP23-388F3, RP23-36D15, RP23-327C12, RP23-235C7), and the Monash Genome Modification Platform (MGMP) and the Australian Phenomics Network (APN) node at Monash University for mouse embryo and blastocyst injections. The APN is supported by the Australian Government Department of Education through the NCRIS, the Super Science Initiative, and the Collaborative Research Infrastructure Scheme. We thank Stefan Siira for assistance with proteomic analyses and James Lingford for technical assistance with yeast experiments.

Author contributions

OR and AF conceived the project. NF, OR, and AF designed the experiments. NF, KLP, DLR, GR, IK, LAH, JAE, LHS, IK, TRR, A-MJS, VKN, LNA, HCS, DT, GCY, LCH, AF, and OR conducted, analyzed, and interpreted the experiments. NF, OR, and AF wrote the manuscript, and the other authors advised and approved the manuscript.

Conflict of interest

The authors declare that they have no conflict of interest.

References

- Agarwal D, Gregory ST, O'Connor M (2011) Error-prone and error-restrictive mutations affecting ribosomal protein S12. *J Mol Biol* 410: 1–9
- Akbergenov R, Duscha S, Fritz AK, Juskeviciene R, Oishi N, Schmitt K, Shcherbakov D, Teo Y, Boukari H, Freihofer P et al (2018) Mutant MRPS5 affects mitoribosomal accuracy and confers stress-related behavioral alterations. *EMBO Rep* 19: e46193
- Amunts A, Brown A, Toots J, Scheres SH, Ramakrishnan V (2015) Ribosome. The structure of the human mitochondrial ribosome. *Science* 348: 95–98
- Bao XR, Ong S-EE, Goldberger O, Peng J, Sharma R, Thompson DA, Vafai SB, Cox AG, Marutani E, Ichinose F et al (2016) Mitochondrial dysfunction remodels one-carbon metabolism in human cells. *eLife* 5: e10575
- Calvo SE, Mootha VK (2010) The mitochondrial proteome and human disease. *Ann Rev Genomics Hum Genet* 11: 25–44
- Cámara Y, Asin-Cayuela J, Park CB, Metodieff MD, Shi Y, Ruzzenente B, Kukat C, Habermann B, Wibom R, Hulthenby K et al (2011) MTERF4 regulates translation by targeting the methyltransferase NSUN4 to the mammalian mitochondrial ribosome. *Cell Metab* 13: 527–539
- Celton-Morizur S, Merlen G, Couton D, Desdouets C (2010) Polyploidy and liver proliferation: central role of insulin signaling. *Cell Cycle* 9: 460–466
- Desai N, Brown A, Amunts A, Ramakrishnan V (2017) The structure of the yeast mitochondrial ribosome. *Science* 355: 528–531
- Ekstrand MI, Falkenberg M, Rantanen A, Park CB, Gaspari M, Hulthenby K, Rustin P, Gustafsson CM, Larsson N-GG (2004) Mitochondrial transcription factor A regulates mtDNA copy number in mammals. *Hum Mol Genet* 13: 935–944
- Gietz R, Woods RA (2006) Yeast transformation by the LiAc/SS Carrier DNA/PEG method. *Methods Mol Biol* 313: 107–120
- Gładych M, Wojtyła A, Rubis B (2011) Human telomerase expression regulation. *Biochem Cell Biol* 89: 359–376
- Glick BS, Pon LA (1995) Isolation of highly purified mitochondria from *Saccharomyces cerevisiae*. *Methods Enzymol* 260: 213–223
- Görner W, Durchschlag E, Wolf J, Brown EL, Ammerer G, Ruis H, Schüller C (2002) Acute glucose starvation activates the nuclear localization signal of a stress-specific yeast transcription factor. *EMBO J* 21: 135–144
- Gouget K, Verde F, Barrientos A (2008) *In vivo* labeling and analysis of mitochondrial translation products in budding and in fission yeasts. *Methods Mol Biol* 457: 113–124
- Greber BJ, Bieri P, Leibundgut M, Leitner A, Aebersold R, Boehringer D, Ban N (2015) The complete structure of the 55S mammalian mitochondrial ribosome. *Science* 348: 303–308
- Greber BJ, Ban N (2016) Structure and function of the mitochondrial ribosome. *Ann Rev Biochem* 85: 103–132
- Hasan R, Leroy C, Isnard A-DD, Labarre J, Boy-Marcotte E, Toledano MB (2002) The control of the yeast H₂O₂ response by the Msn2/4 transcription factors. *Mol Microbiol* 45: 233–241
- Higuchi-Sanabria R, Frankino PA, Paul JW, Tronnes SU, Dillin A (2018) A futile battle? Protein quality control and the stress of aging. *Dev Cell* 44: 139–163
- Houtkooper RH, Mouchiroud L, Ryu D, Moullan N, Katsyuba E, Knott G, Williams RW, Auwerx J (2013) Mitonuclear protein imbalance as a conserved longevity mechanism. *Nature* 497: 451–457
- Huang DW, Sherman BT, Lempicki RA (2009) Systematic and integrative analysis of large gene lists using DAVID bioinformatics resources. *Nat Protoc* 4: 44–57
- Jiang M, Kauppila TE, Motori E, Li X, Atanassov I, Folz-Donahue K, Bonekamp NA, Albarran-Gutierrez S, Stewart JB, Larsson N-GG (2017) Increased total mtDNA copy number cures male infertility despite unaltered mtDNA mutation load. *Cell Metab* 26: 429–436.e4
- Kandror O, Bretschneider N, Kreydin E, Cavaliere D, Goldberg AL (2004) Yeast adapt to near-freezing temperatures by STRE/Msn2,4-dependent induction of trehalose synthesis and certain molecular chaperones. *Mol Cell* 13: 771–781
- Kolde R (2019) pheatmap: Pretty Heatmaps. R package version 1.0.12. <https://CRAN.R-project.org/package=pheatmap>
- Kreutz C, MacNelly S, Follo M, Wäldin A, Binnering-Lacour P, Timmer J, Bartolomé-Rodríguez MM (2017) Hepatocyte ploidy is a diversity factor for liver homeostasis. *Front Physiol* 8: 862
- Kühl I, Miranda M, Atanassov I, Kuznetsova I, Hinze Y, Mourier A, Filipovska A, Larsson N-GG (2017) Transcriptomic and proteomic landscape of mitochondrial dysfunction reveals secondary coenzyme Q deficiency in mammals. *eLife* 6: e30952
- Kummer E, Leibundgut M, Rackham O, Lee RG, Boehringer D, Filipovska A, Ban N (2018) Unique features of mammalian mitochondrial translation initiation revealed by cryo-EM. *Nature* 560: 263–267
- Kuznetsova I, Lugmayr A, Siira SJ, Rackham O, Filipovska A (2019) CirGO: an alternative circular way of visualising gene ontology terms. *BMC Bioinformatics* 20: 84
- Lin S, Nascimento EM, Gajera CR, Chen L, Neuhöfer P, Garbuzov A, Wang S, Artandi SE (2018) Distributed hepatocytes expressing telomerase repopulate the liver in homeostasis and injury. *Nature* 556: 244–248
- Moehle EA, Shen K, Dillin A (2018) Mitochondrial proteostasis in the context of cellular and organismal health and aging. *J Biol Chem* 294: 5396–5407
- Mohler K, Ibbá M (2017) Translational fidelity and mistranslation in the cellular response to stress. *Nat Microbiol* 2: 17117
- Morita M, Gravel S-PP, Chénard V, Sikström K, Zheng L, Alain T, Gandin V, Avizonis D, Arguello M, Zakaria C et al (2013) mTORC1 controls

- mitochondrial activity and biogenesis through 4E-BP-dependent translational regulation. *Cell Metab* 18: 698–711
- Moura GR, Carreto LC, Santos MA (2009) Genetic code ambiguity: an unexpected source of proteome innovation and phenotypic diversity. *Curr Opin Microbiol* 12: 631–637
- Mourier A, Matic S, Ruzzenente B, Larsson N-GG, Milenkovic D (2014) The respiratory chain supercomplex organization is independent of COX7a2 isoforms. *Cell Metab* 20: 1069–1075
- Münch C, Harper J (2016) Mitochondrial unfolded protein response controls matrix pre-RNA processing and translation. *Nature* 534: 710–713
- Murphy MP, Hartley RC (2018) Mitochondria as a therapeutic target for common pathologies. *Nat Rev Drug Discov* 17: 865–886
- Netzer N, Goodenbour JM, David A, Dittmar KA, Jones RB, Schneider JR, Boone D, Eves EM, Rosner MR, Gibbs JS et al (2009) Innate immune and chemically triggered oxidative stress modifies translational fidelity. *Nature* 462: 522–526
- Owen OE, Kalhan SC, Hanson RW (2002) The key role of anaplerosis and cataplerosis for citric acid cycle function. *J Biol Chem* 277: 30409–30412
- Pagliarini DJ, Rutter J (2013) Hallmarks of a new era in mitochondrial biochemistry. *Genes Dev* 27: 2615–2627
- Pareek G, Thomas RE, Vincow ES, Morris DR, Pallanck LJ (2018) Lon protease inactivation in *Drosophila* causes unfolded protein stress and inhibition of mitochondrial translation. *Cell Death Discov* 4: 51
- Park CB, Asin-Cayuela J, Cámara Y, Shi Y, Pellegrini M, Gaspari M, Wibom R, Hultenby K, Erdjument-Bromage H, Tempst P et al (2007) MTERF3 is a negative regulator of mammalian mtDNA transcription. *Cell* 130: 273–285
- Parker J (1989) Errors and alternatives in reading the universal genetic code. *Microbiol Rev* 53: 273–298
- Parlo RA, Coleman PS (1984) Enhanced rate of citrate export from cholesterol-rich hepatoma mitochondria. The truncated Krebs cycle and other metabolic ramifications of mitochondrial membrane cholesterol. *J Biol Chem* 259: 9997–10003
- Perks KL, Ferreira N, Richman TR, Ermer JA, Kuznetsova I, Shearwood A-MJ, Lee RG, Viola HM, Johnstone VP, Matthews V et al (2017) Adult-onset obesity is triggered by impaired mitochondrial gene expression. *Sci Adv* 3: e1700677
- Perks KL, Rossetti G, Kuznetsova I, Hughes LA, Ermer JA, Ferreira N, Busch JD, Rudler DL, Spahr H, Schöndorf T et al (2018) PTC1 is required for 16S rRNA maturation complex stability and mitochondrial ribosome assembly. *Cell Rep* 23: 127–142
- Presnyak V, Alhusaini N, Chen Y-HH, Martin S, Morris N, Kline N, Olson S, Weinberg D, Baker KE, Graveley BR et al (2015) Codon optimality is a major determinant of mRNA stability. *Cell* 160: 1111–1124
- Quiros PM, Langer T, López-Otín C (2015) New roles for mitochondrial proteases in health, ageing and disease. *Nat Rev Mol Cell Biol* 16: 345–359
- Rackham O, Busch JD, Matic S, Siira SJ, Kuznetsova I, Atanassov I, Ermer JA, Shearwood A-MJ, Richman TR, Stewart JB et al (2016) Hierarchical RNA processing is required for mitochondrial ribosome assembly. *Cell Rep* 16: 1874–1890
- Richman TR, Ermer JA, Davies S, Perks KL, Viola HM, Shearwood AM, Hool LC, Rackham O, Filipovska A (2015) Mutation in MRPS34 compromises protein synthesis and causes mitochondrial dysfunction. *PLoS Genet* 11: e1005089
- Richman TR, Spähr H, Ermer JA, Davies S, Viola HM, Bates KA, Papadimitriou J, Hool LC, Rodger J, Larsson N-GG et al (2016) Loss of the RNA-binding protein TACO1 causes late-onset mitochondrial dysfunction in mice. *Nat Commun* 7: 11884
- Riera CE, Merkwirth C, Filho DC, Dillin A (2016) Signaling networks determining life span. *Ann Rev Biochem* 85: 35–64
- Ruzzenente B, Metodiev MD, Wredenberg A, Bratic A, Park CB, Cámara Y, Milenkovic D, Zickermann V, Wibom R, Hultenby K et al (2012) LRPPRC is necessary for polyadenylation and coordination of translation of mitochondrial mRNAs. *EMBO J* 31: 443–456
- Sasaman F, Antonicka H, Shoubridge EA (2008) The A3243G tRNA^{Leu}(UUR) MELAS mutation causes amino acid misincorporation and a combined respiratory chain assembly defect partially suppressed by overexpression of EFTu and EFG2. *Hum Mol Genet* 17: 3697–3707
- Satapati S, Sunny NE, Kucejova B, Fu X, He TT, Méndez-Lucas A, Shelton JM, Perales JC, Browning JD, Burgess SC (2012) Elevated TCA cycle function in the pathology of diet-induced hepatic insulin resistance and fatty liver. *J Lipid Res* 53: 1080–1092
- Seiferling D, Szczepanowska K, Becker C, Senft K, Hermans S, Maiti P, König T, Kukat A, Trifunovic A (2016) Loss of CLPP alleviates mitochondrial cardiomyopathy without affecting the mammalian UP^{mt}. *EMBO Rep* 17: 953–964
- Small ID, Rackham O, Filipovska A (2013) Organelle transcriptomes: products of a deconstructed genome. *Curr Opin Microbiol* 16: 652–658
- Suhm T, Kaimal JM, Dawitz H, Peselj C, Masser AE, Hanzén S, Ambrožič M, Smialowska A, Björck ML, Brzezinski P et al (2018) Mitochondrial translation efficiency controls cytoplasmic protein homeostasis. *Cell Metab* 27: 1309–1322
- Supek F, Bošnjak M, Škunca N, Šmuc T (2011) REVIGO summarizes and visualizes long lists of Gene Ontology terms. *PLoS ONE* 6: e21800
- Suzuki T, Nagao A, Suzuki T (2011) Human mitochondrial tRNAs: biogenesis, function, structural aspects, and diseases. *Annu Rev Genet* 45: 299–329
- Svenningsen SL, Kongstad M, Stenum TS, Muñoz-Gómez AJ, Sørensen MA (2017) Transfer RNA is highly unstable during early amino acid starvation in *Escherichia coli*. *Nucleic Acids Res* 45: 793–804
- Vafai SB, Mootha VK (2012) Mitochondrial disorders as windows into an ancient organelle. *Nature* 491: 374–383
- Wang G, Wang Q, Huang Q, Chen Y, Sun X, He L, Zhan L, Guo X, Yin C, Fang Y et al (2018) Upregulation of mtSSB by interleukin-6 promotes cell growth through mitochondrial biogenesis-mediated telomerase activation in colorectal cancer. *Int J Cancer* 144: 2516–2528
- Wohlgemuth I, Pohl C, Rodnina MV (2010) Optimization of speed and accuracy of decoding in translation. *EMBO J* 29: 3701–3709
- Zaher HS, Green R (2009) Fidelity at the molecular level: lessons from protein synthesis. *Cell* 136: 746–762
- Zhang G, Ignatova Z (2010) Folding at the birth of the nascent chain: coordinating translation with co-translational folding. *Curr Opin Struct Biol* 21: 25–31
- Zhao Q, Wang J, Levichkin IV, Stasinopoulos S, Ryan MT, Hoogenraad NJ (2002) A mitochondrial specific stress response in mammalian cells. *EMBO J* 21: 4411–4419